Inelastic quantum Boltzmann equation of single-component Fermi gases

Xin-Yuan Gao[1] and Yangqian Yan[1,2,*]

[1]*Department of Physics, The Chinese University of Hong Kong, Shatin, New Territories, Hong Kong, China*

[2]*The Chinese University of Hong Kong Shenzhen Research Institute, 518057 Shenzhen, China*

(Received 23 October 2024; revised 13 February 2025; accepted 21 March 2025; published 17 April 2025)

This work is a companion paper to X.-Y. Gao *et al.*, Phys. Rev. Lett. **134**, 153402 (2025), where we discuss the nonequilibrium two-body loss dynamics of a single-component ultracold Fermi gas and its possible thermalization. This paper provides detailed information on the derivation and analysis of the inelastic quantum Boltzmann equation (IQBE) used to describe the system. We demonstrate that the Mellin transform is a powerful tool for solving and approximating the IQBE for free-space systems. In this case, the particle-number dynamics are beyond the description of the widely used phenomenological two-body equation. For harmonically trapped systems, we propose a fast-flowing approximation to simplify the numerical evaluation of the IQBE. We verify the approximation in an analogous quasi-one-dimensional system and apply it to three-dimensional calculations, obtaining satisfactory agreement with recent experimental results. Furthermore, we compare the nonequilibrium results with those obtained using a thermal ansatz in both situations, providing a systematic understanding of the antievaporation phenomena observed in such systems.

DOI: 10.1103/PhysRevA.111.043312

I. INTRODUCTION

As the key concept in the kinetic theory, the Boltzmann equation describes the evolution of a classic many-body system towards thermal equilibrium [1]. An analog can be obtained for normal-phase quantum gases or even Bose-Einstein condensates [2] and fermionic superfluid [3,4], known as the quantum Boltzmann equation. It is notoriously hard to solve such equations directly due to their six-dimensional spatial complexity and the sophisticated form of the collision integral. Under the collision integral's relaxation approximation (or Bhatnagar-Gross-Krook (BGK) approximation [5]), the Boltzmann equation has been widely adopted to study hydrodynamic expansion [6,7], collective modes [8,9], and spin waves [10] in harmonically trapped quantum gases. Various numerical methods also tackle collision integral without approximation, mainly based on the direct simulation Monte Carlo method [11,12] and its variants [13–17]. In all usual applications above, the particles are assumed to be featureless and only possess translational motions. Consequently, the collision integral only captures the system's elastic collisions. However, inelastic collisions can also play an essential role in certain situations, especially in the study of ultracold molecular gases, where the inelastic collision due to intrinsic chemical reactions affects the efficiency of evaporative cooling and the lifetime of the gas [18]. In the Boltzmann equations describing classic granular fluids, the inelastic collision is implemented by breaking momentum and energy conservation in the collision integral [19–23]. Nevertheless, such generalization cannot be directly applied to quantum Boltzmann equations since the inelastic collision changes the particles' internal states, which indicates not only the dissipation of energy but also the loss of the total number of particles (if we only concern the internal states where particles start from). Note that non-Hermitian linear response theory predicts (stretched) exponential loss for a one-body loss and broadening of momentum distribution for two-body atom-number-conserving dissipation in a short timescale [24]. In comparison, this work considers the long-time dynamics as well as the effect of the two-body lossy dissipator.

In this article (and corresponding Letter [25]), we focus on single-component ultracold molecular Fermi gas, a simple but highly nontrivial quantum gas system with inelastic collision, to demonstrate how to model the system's dynamics with a proper inelastic quantum Boltzmann equation (IQBE). Experimentally, this is related to two molecular platforms, including ^{40}K ^{87}Rb (e.g., see Ref. [26]) and ^{23}Na ^{40}K (e.g., see Ref. [27]) Fermi gases with two-body loss induced by chemical reactions and two atomic platforms: Li and K with two-body loss induced by dipolar relaxation. Here are some general properties of those systems: (i) Although the detailed mechanism may differ, the outcomes are the same. The outgoing particles of inelastic scattering will gain enough kinetic energy to escape from the trap. As a result, two particles will be lost per inelastic collision event. (ii) The systems are prepared with initial temperatures typically below 1 μK. In this ultracold regime, the two-body collision follows threshold behavior, i.e., only the lowest possible partial wave channel dominates the phase shift. This is true for both elastic and inelastic collisions. (iii) Unlike the usual Fermi gas with balanced spin-up and -down components, all particles in such systems are typically prepared in the same rovibrational ground state. Because of the Pauli exclusion principle, the natural lowest partial wave channel, *s*-wave collision, is prohibited. Combined with the above mentioned, the *p*-wave channel will dominate,

*Contact author: yqyan@cuhk.edu.hk

providing the interparticle potential with a centrifugal barrier. As detailed in this work, the relative momentum selection caused by the centrifugal barrier is the origin of the intriguing dynamics of such systems. (iv) Without Feshbach resonance, the bare scattering volume of elastic collision is extremely small. Furthermore, when the system is away from the equilibrium state, p-wave collision cannot equilibrate the system in a typical experimental timescale. The argument will also be elaborated in the following sections.

This work will be mainly divided into three parts. In the first part, we introduce the model, derive the IQBE from scratch, and comment on the system's relaxation time. In the second part, we focus on homogeneous systems with spatial translational symmetry. In the third part, we work on harmonically trapped systems closely related to recent experiments.

II. NON-HERMITIAN HAMILTONIAN

As explained in Sec. I, we must construct a model with p-wave interaction and include inelastic collision. The simplest option is to use one-channel non-Hermitian Hamiltonian

$$\begin{aligned}\hat{H} &= \hat{T} + \hat{U},\\ \hat{T} &= \sum_{\mathbf{k}} \frac{\hbar^2 k^2}{2M} c_{\mathbf{k}}^\dagger c_{\mathbf{k}},\\ \hat{U} &= \frac{3g}{2V} \sum_{\mathbf{P},\mathbf{q},\mathbf{q}'} \mathbf{q}\cdot\mathbf{q}' c^\dagger_{\frac{\mathbf{P}}{2}+\mathbf{q}} c^\dagger_{\frac{\mathbf{P}}{2}-\mathbf{q}} c_{\frac{\mathbf{P}}{2}-\mathbf{q}'} c_{\frac{\mathbf{P}}{2}+\mathbf{q}'},\end{aligned} \tag{1}$$

where M is the mass of particles, V the volume of the system, and $c_{\mathbf{k}}$ the annihilation operator of a particle. The momentum dependence in the interaction reflects the p-wave symmetry. Importantly, the coupling constant g is a complex number, accounting for both elastic and inelastic collisions. The non-Hermitian Hamiltonian here is an effective field theory from a Hermitian model, integrating the product channel of two-body chemical reaction [28]. For low-temperature threshold collision, the phase shift of the p-wave channel δ_p can be expanded as $k^3\cot(\delta_p) = -1/v_p + O(k^2)$, where v_p is defined as the scattering volume. Because the system has inelastic collisions, both δ_p and v_p are expected to be complex. Following the standard renormalization procedure of comparing T matrix calculated from Eq. (1) with scattering amplitude, one has

$$\frac{1}{g} = \frac{M}{4\pi\hbar^2 v_p} + \frac{M}{2\pi^2\hbar^2}\int_0^\infty dq\, q^2. \tag{2}$$

In this work, we treat the scattering volume to be small and far from any p-wave resonance, thus, it is enough only to take the normal part of the renormalization condition, which is

$$g = 4\pi\hbar^2[\mathrm{Re}(v_p) + i\,\mathrm{Im}(v_p)]/M. \tag{3}$$

Most literature discussing many-body systems with p-wave collision stresses the importance of effective range R aside from v_p. It is defined through the next-order expansion of p-wave phase shift $k^3\cot(\delta_p) = -1/v_p - k^2/R + O(k^4)$. In the following discussion, for simplicity of application to typical ultracold molecular or atomic systems, we focus on conditions under which the term involving R is subdominant. Explicitly, the application range for our theory is

$$n^{5/3}\left|\frac{v_p^2}{R}\right| \ll n\,|v_p| \ll 1, \tag{4}$$

where n is the number density. This set of inequalities is motivated by the "naturalness" of the systems in question, in which the scattering volume v_p and the effective range R arise from the same underlying van der Waals potential. Specifically, we denote $\ell \simeq v_p^{1/3}$ as the natural length scale associated with the van der Waals coefficient C_6, and we assume $n \ll \ell^{-3}$. Consequently, one finds

$$n^{5/3}\left(\frac{v_p^2}{R}\right) \sim n^{5/3}\,\ell^5 \sim n^{2/3}\,\ell^2\,(n\,v_p) \ll n\,v_p \ll 1,$$

thus justifying the neglect of the effective range in most cases considered here. As a concrete example, for ^{40}K atoms in the ground state, one has $v_p \simeq (96.74\,a_0)^3$ and $R \simeq 46.22\,a_0$ [29,30], meaning $\ell \equiv v_p^{1/3}$ and R differ by only about a factor of 0.48, illustrating that the length scales are indeed comparable. However, we should emphasize that the argument does not completely exclude the extreme case: if a particular system were to realize extremely small R at a given v_p, one might need to include the effective-range corrections for a more accurate description.

III. INELASTIC QUANTUM BOLTZMANN EQUATION

In this section, we provide a deviation of the inelastic quantum Boltzmann equation we will use to describe the dissipation dynamics in this work. The standard form of a Boltzmann equation is an equation of motion of phase-space density $f(\mathbf{k},\mathbf{r})$, composed of Vlasov equation for modeling diffusion and drift flow and collision integral $\mathcal{I}_{\mathrm{coll}}[f]$ depicting the collision

$$\frac{df}{dt} + \left[\frac{\hbar\mathbf{k}}{M}\nabla_{\mathbf{r}} - \frac{\nabla_{\mathbf{r}}U_{\mathrm{ext}}\cdot\nabla_{\mathbf{k}}}{\hbar}\right]f = \mathcal{I}_{\mathrm{coll}}[f]. \tag{5}$$

The task is to obtain the form of $\mathcal{I}_{\mathrm{coll}}[f]$ from the first principle, e.g., the Schrödinger equation.

We start with homogeneous systems, where we assume $f(\mathbf{k},\mathbf{r}) = V n_{\mathbf{k}}$ with $n_{\mathbf{k}}$ the momentum distribution of the system. It simplifies Eq. (5) to

$$\frac{dn_{\mathbf{k}}}{dt} = \frac{1}{V}\mathcal{I}_{\mathrm{coll}}[V n_{\mathbf{k}}]. \tag{6}$$

After obtaining $\mathcal{I}_{\mathrm{coll}}[V n_{\mathbf{k}}]/V$ for homogeneous systems, we immediately have the form $\mathcal{I}_{\mathrm{coll}}$ which also applied to the arbitrary inhomogeneous system under local density approximation, which means one treats each local regimes a separate small homogeneous piece. The approximation is exact in the thermodynamic limit.

We use the following symbols to denote the time dependence of operators, states, and the density matrix in different pictures:

Schrödinger picture: $\hat{A}$, $|\psi_t\rangle$, ρ_t;

Heisenburg picture: $\hat{A}_t$, $|\psi\rangle$, ρ;

Interaction picture: $\hat{A}(t)$, $|\psi(t)\rangle$.

Investigating the evolution of $n_{\mathbf{k}}$ is equivalent to studying the dynamics of number operator $N_{\mathbf{k}} = c_{\mathbf{k}}^{\dagger} c_{\mathbf{k}}$. In a small time window t, the change of expectation $\langle N_{\mathbf{k}} \rangle$ is

$$\begin{aligned}\Delta\langle N_{\mathbf{k}}\rangle &= \mathrm{Tr}(\rho_t N_{\mathbf{k}}) - \mathrm{Tr}(\rho_0 N_{\mathbf{k}}) \\ &= \sum_n \rho_{nn}[\langle n(t)|N_{\mathbf{k}}|n(t)\rangle - \langle n_0|N_{\mathbf{k}}|n_0\rangle] \\ &= \sum_n \rho_{nn}\langle n|e^{\frac{i}{\hbar}\mathcal{T}\int \hat{U}^{\dagger}(t)dt} \\ &\quad \times \left(N_{\mathbf{k}} e^{-\frac{i}{\hbar}\mathcal{T}\int^t \hat{U}(t')dt'} - e^{-\frac{i}{\hbar}\mathcal{T}\int^t \hat{U}^{\dagger}(t')dt'} N_{\mathbf{k}}\right)|n\rangle. \quad (7)\end{aligned}$$

Here, we use the symbol $|n\rangle$ to denote a general Fock state, and $\mathcal{T}$ is the time-ordered operator. Based on the definition of $\mathcal{T}$ [31], one can expand $\Delta\langle N_{\mathbf{k}}\rangle$ up to the second-order in terms of the interaction

$$\Delta\langle N_{\mathbf{k}}\rangle = \Delta\langle N_{\mathbf{k}}\rangle^{(1)} + \Delta\langle N_{\mathbf{k}}\rangle_1^{(2)} + \Delta\langle N_{\mathbf{k}}\rangle_2^{(2)}, \quad (8)$$

where the first-order term is

$$\langle N_{\mathbf{k}}\rangle^{(1)} = \sum_n \frac{\rho_{nn}}{i\hbar}\langle n|N_{\mathbf{k}}\int_0^t \hat{U}(t')dt' - \int_0^t \hat{U}^{\dagger}(t')dt' N_{\mathbf{k}}|n\rangle. \quad (9)$$

And there are two second-order terms, which are

$$\begin{aligned}\Delta\langle N_{\mathbf{k}}\rangle_1^{(2)} &= \sum_n \frac{\rho_{nn}}{\hbar^2}\langle n|\int_0^t \hat{U}^{\dagger}(t')dt' \\ &\quad \times \left(N_{\mathbf{k}}\int_0^t \hat{U}(t')dt' - \int_0^t \hat{U}^{\dagger}(t')dt' N_{\mathbf{k}}\right)|n\rangle \quad (10)\end{aligned}$$

and

$$\begin{aligned}\Delta\langle N_{\mathbf{k}}\rangle_2^{(2)} &= -\sum_n \frac{\rho_{nn}}{\hbar^2}\langle n|N_{\mathbf{k}}\int_0^t dt'\int_0^{t'} dt''\hat{U}(t')\hat{U}(t'') \\ &\quad - \int_0^t dt'\int_0^{t'} dt''\hat{U}^{\dagger}(t')\hat{U}^{\dagger}(t'')N_{\mathbf{k}}|n\rangle. \quad (11)\end{aligned}$$

It is worth emphasizing that since $\hat{U}$ is non-Hermitian, $\hat{U}^{\dagger}$ is distinguishable from $\hat{U}$. The expansion up to the second order is justified by the fact that interaction is weak enough, which will be further confirmed in Sec. IV.

Let us focus on the $\langle N_{\mathbf{k}}\rangle^{(1)}$ first. Decomposing the term by separating real and imaginary parts of interaction and taking the short-time limit, we have

$$\begin{aligned}\Delta\langle N_{\mathbf{k}}\rangle^{(1)} &\xrightarrow{t\to 0} \frac{t}{i\hbar}\sum_n \rho_{nn}\langle n|[N_{\mathbf{k}}, \mathrm{Re}(\hat{U})]|n\rangle \\ &\quad + \frac{t}{\hbar}\sum_n \rho_{nn}\langle n|\{N_{\mathbf{k}}, \mathrm{Im}(\hat{U})\}|n\rangle. \quad (12)\end{aligned}$$

Before further proceeding, an important observation is that the second term above is not physical since if we replace $N_{\mathbf{k}}$ with identity operator $\mathbb{I}$ (in the previous steps, we do not explicitly use the form of $N_{\mathbf{k}}$, so this is available),

$$\Delta\langle\mathbb{I}\rangle^{(1)} = \Delta\,\mathrm{Tr}(\rho) \stackrel{?}{=} \frac{2t}{\hbar}\mathrm{Im}(\hat{U}). \quad (13)$$

Because the trace of the density matrix should always be one, $\Delta\,\mathrm{Tr}(\rho) = 0$, which is inconsistent with the right-hand side of the equation. To fix the problem, we should artificially add a Lindblad jump term to Eq. (12),

$$\begin{aligned}\Delta\langle N_{\mathbf{k}}\rangle^{(1)} &= \frac{t}{i\hbar}\sum_n \rho_{nn}\langle n|[N_{\mathbf{k}}, \mathrm{Re}(\hat{U})]|n\rangle \\ &\quad + \frac{t}{\hbar}\sum_n \rho_{nn}\langle n|\{N_{\mathbf{k}}, \mathrm{Im}(\hat{U})\}|n\rangle \\ &\quad - \frac{2t}{\hbar}\sum_{n,\mathbf{P},m} \rho_{nn}\langle n|\hat{L}_{\mathbf{P},m}^{\dagger} N_{\mathbf{k}}\hat{L}_{\mathbf{P},m}|n\rangle, \quad (14)\end{aligned}$$

where $\sum_{\mathbf{P},m} L_{\mathbf{P},m}^{\dagger} L_{\mathbf{P},m} = \mathrm{Im}(\hat{U})$. One can check that if $N_{\mathbf{k}}$ is replaced by identity operator $\mathbb{I}$ in Eq. (14), the trace of the density matrix is conserved. To find the form of $L_{\mathbf{P},m}$, we use the addition theorem of Legendre polynomial,

$$\mathbf{q}\cdot\mathbf{q}' = qq' P_1(\hat{\mathbf{q}}\cdot\hat{\mathbf{q}}') = \frac{4\pi}{3}\sum_{m=-1}^{l} Y_{1m}(\hat{\mathbf{q}})Y_{1m}^*(\hat{\mathbf{q}}'), \quad (15)$$

where Y_{lm} are the spherical harmonics. Combining with Eq. (1), we read off that the explicit form of $L_{\mathbf{P},m}$ is

$$\hat{L}_{\mathbf{P},m} = \sum_{\mathbf{q}} 2\sqrt{\pi\,\mathrm{Im}(g)}qY_{1m}(\hat{\mathbf{q}})c_{\frac{\mathbf{P}}{2}-\mathbf{q}}c_{\frac{\mathbf{P}}{2}+\mathbf{q}}. \quad (16)$$

Then, a straightforward while lengthy calculation gives

$$\begin{aligned}\Delta\langle N_{\mathbf{k}}\rangle^{(1)} &= -\frac{6t}{\hbar V}\sum_n \rho_{nn}\sum_{\mathbf{P},\mathbf{q}}\left(\mathbf{q}-\frac{\mathbf{P}}{2}\right)\cdot\left(\mathbf{k}-\frac{\mathbf{P}}{2}\right) \\ &\quad \times [\mathrm{Re}(g)\mathrm{Im}\langle n|c_{\mathbf{k}}^{\dagger}c_{\mathbf{P}-\mathbf{k}}^{\dagger}c_{\mathbf{q}}c_{\mathbf{P}-\mathbf{q}}|n\rangle \\ &\quad + \mathrm{Im}(g)\mathrm{Re}\langle n|c_{\mathbf{k}}^{\dagger}c_{\mathbf{P}-\mathbf{k}}^{\dagger}c_{\mathbf{q}}c_{\mathbf{P}-\mathbf{q}}|n\rangle]. \quad (17)\end{aligned}$$

Recalling that we choose $|n\rangle$ to represent Fock states, the expectation can be evaluated following the canonical anticommutation relation

$$\begin{aligned}&\langle n|c_{\mathbf{k}}^{\dagger}c_{\mathbf{P}-\mathbf{k}}^{\dagger}c_{\mathbf{q}}c_{\mathbf{P}-\mathbf{q}}|n\rangle \\ &\quad = (1-\delta_{\mathbf{q},\mathbf{P}/2})(\delta_{\mathbf{q}+\mathbf{k},\mathbf{P}} - \delta_{\mathbf{q},\mathbf{k}})N_{\mathbf{k}}(n)N_{\mathbf{P}-\mathbf{k}}(n) \\ &\quad + \delta_{\mathbf{q},\mathbf{P}/2}\delta_{\mathbf{k},\mathbf{P}/2}N_{\mathbf{k}}(n)[N_{\mathbf{k}}(n)-1], \quad (18)\end{aligned}$$

where $N_{\mathbf{k}}(n)$ signifies occupation number of particle with momentum $\mathbf{k}$ of state $|n\rangle$. Substituting the above result to Eq. (17), we have

$$\begin{aligned}\frac{\Delta\langle N_{\mathbf{k}}^{(1)}\rangle}{t} &\xrightarrow{t\to 0} \frac{d\langle N_{\mathbf{k}}\rangle^{(1)}}{dt} \\ &= -\frac{6\,\mathrm{Im}(g)}{\hbar V}\sum_n \rho_{nn}\sum_{\mathbf{P},\mathbf{q}}\left(\mathbf{q}-\frac{\mathbf{P}}{2}\right)\cdot\left(\mathbf{k}-\frac{\mathbf{P}}{2}\right) \\ &\quad \times (\delta_{\mathbf{q}+\mathbf{k},\mathbf{P}} - \delta_{\mathbf{q},\mathbf{k}})N_{\mathbf{k}}(n)N_{\mathbf{P}-\mathbf{k}}(n). \quad (19)\end{aligned}$$

Changing variable $\mathbf{P}\to\mathbf{q}'+\mathbf{k}$, one observes that two delta functions contribute equally:

$$\frac{d\langle N_{\mathbf{k}}\rangle^{(1)}}{dt} = \frac{3\,\mathrm{Im}(g)}{\hbar V}\sum_n \rho_{nn}\sum_{\mathbf{q}}(\mathbf{q}-\mathbf{k})^2 N_{\mathbf{k}}(n)N_{\mathbf{q}}(n). \quad (20)$$

Because we assume that the interaction of the system is weak, to the leading order, the expectation of $N_{\mathbf{k}}$ and $N_{\mathbf{q}}$ can be

factorized [32]:

$$\frac{d\langle N_{\mathbf{k}}\rangle^{(1)}}{dt} = \frac{3\,\mathrm{Im}(g)}{\hbar V}\sum_{n,n'}\rho_{nn}\rho_{n'n'}\sum_{\mathbf{q}}(\mathbf{q}-\mathbf{k})^2 N_{\mathbf{k}}(n)N_{\mathbf{q}}(n') = \frac{3\,\mathrm{Im}(g)}{\hbar}\int\frac{d^3q}{(2\pi)^3}(\mathbf{q}-\mathbf{k})^2\langle N_{\mathbf{k}}\rangle\langle N_{\mathbf{q}}\rangle. \tag{21}$$

It is noted that the right-hand side of Eq. (21) has already given a part of $\mathcal{I}_{\mathrm{coll}}[Vn_{\mathbf{k}}]/V$. Utilizing the spherical symmetry of $\langle N_{\mathbf{k}}\rangle$ (it has the symmetry because the interaction $\hat{U}$ here is spherical symmetric) and $\langle N_{\mathbf{k}}\rangle = Vn_{\mathbf{k}}$:

$$\mathcal{I}_{\mathrm{coll}}[Vn_{\mathbf{k}}]/V = \mathcal{I}_{\mathrm{inel}}[Vn_{\mathbf{k}}]/V + \cdots = \frac{12\pi\hbar\,\mathrm{Im}(v_p)V}{M}\int\frac{d^3q}{(2\pi)^3}(q^2+k^2)n_{\mathbf{k}}n_{\mathbf{q}} + \cdots. \tag{22}$$

One observes that this part of the collision integral neither has a constraint on momentum or energy conservation nor a parameter related to $\mathrm{Re}(v_p)$; thus, it is not a conventional collision integral characterizing the strength of elastic collision, but a part describing the momentum dependence of two-body chemical reaction. We name this part of $\mathcal{I}_{\mathrm{coll}}$ to be $\mathcal{I}_{\mathrm{inel}}$, the inelastic collision integral. An equivalence of Eq. (22) has first been obtained by Ref. [33] using a two-channel model. Here, we derive Eq. (22) using our one-channel model differently to make symbols self-contained. It is worth noting that although reaching a similar Eq. (22), our following analysis is distinct from that in Ref. [33], especially for the harmonically trapped scenario. There are even more different methods for arriving at an inelastic collision integral in a two-body dissipative system. For example, Refs. [24,34,35] reach similar equations using linear response theory and Keldysh field theory, respectively. In Appendix A, we also show that if one is not concerned about elastic collision completely, it is also convenient to derive the inelastic collision integral (22) directly from the Lindblad master equation.

We find that up to the first-order expansion, only inelastic collision is considered. One needs to go to the second-order expansion to account for elastic collision. Since we assume interaction and reaction are weak, we ignore all inelastic collision contributions from the second-order process. Consequently, when consider the second-order process, we take $\hat{U}(t) = \hat{U}(t)^\dagger = \mathrm{Re}[\hat{U}(t)]$. Reference [32] argues that only $\Delta\langle N_{\mathbf{k}}\rangle_1^{(2)}$ contributes to the collision integral. With the simplification above,

$$\Delta\langle N_{\mathbf{k}}\rangle^{(2)} = \Delta\langle N_{\mathbf{k}}\rangle_1^{(2)} = \sum_n\frac{\rho_{nn}}{\hbar^2}\langle n|\int_0^t\int_0^t dt'dt''\mathrm{Re}[\hat{U}(t)][N_{\mathbf{k}},\mathrm{Re}[\hat{U}(t)]]|n\rangle = \sum_{n,l}\rho_{nn}\frac{\sin^2[(E_n-E_l)t/2\hbar]}{(E_n-E_l)^2}\langle n|\mathrm{Re}(\hat{U})|l\rangle\langle l|[N_{\mathbf{k}},\mathrm{Re}(\hat{U})]|n\rangle, \tag{23}$$

where E_n and E_l denote energy of state $|n\rangle$ and $|l\rangle$, respectively. Taking the Markovian limit for the above expression [32], we have

$$\Delta\langle N_{\mathbf{k}}\rangle^{(2)} = \frac{2\pi t}{\hbar}\sum_{n,l}\rho_{nn}\delta(E_n-E_l)\langle n|\mathrm{Re}(\hat{U})|l\rangle\langle l|[N_{\mathbf{k}},\mathrm{Re}(\hat{U})]|n\rangle. \tag{24}$$

Because both $|n\rangle$ and $|l\rangle$ are Fock states, it is possible to directly evaluate expectations in Eq. (24), which yields

$$\begin{aligned}\sum_{n,l}\rho_{nn}\langle n|\mathrm{Re}(\hat{U})|l\rangle\langle l|[N_{\mathbf{k}},\mathrm{Re}(\hat{U})]|n\rangle = \frac{9}{2}\frac{\mathrm{Re}(g)^2}{V^2}\sum_{\mathbf{P},\mathbf{Q},\mathbf{p},\mathbf{p}',\mathbf{q}}(\mathbf{p}\cdot\mathbf{p}')\left[\left(\frac{\mathbf{Q}}{2}-\mathbf{k}\right)\cdot\mathbf{q}\right][\delta_{\mathbf{p},\mathbf{q}}\delta_{\mathbf{P},\mathbf{Q}}\delta_{\mathbf{P}/2+\mathbf{p}',\mathbf{k}}(1-\langle N_{\mathbf{Q}-\mathbf{k}}\rangle)\\ \times(1-\langle N_{\mathbf{k}}\rangle)N_{\mathbf{Q}/2-\mathbf{q}}N_{\mathbf{Q}/2+\mathbf{q}} - \delta_{\mathbf{p}',\mathbf{q}}\delta_{\mathbf{P},\mathbf{Q}}\delta_{\mathbf{P}/2-\mathbf{p},\mathbf{k}}(1-\langle N_{\mathbf{Q}/2+\mathbf{q}}\rangle)\\ \times(1-\langle N_{\mathbf{Q}/2-\mathbf{q}}\rangle)N_{\mathbf{k}}N_{\mathbf{Q}-\mathbf{k}}].\end{aligned} \tag{25}$$

Again, we factorize expectations of the number of particles with different momentum as what is done in Eq. (18). Combining Eqs. (24) and (25), we have

$$\begin{aligned}\frac{\Delta\langle N_{\mathbf{k}}\rangle^{(2)}}{t}\xrightarrow{t\to 0}\frac{d\langle N_{\mathbf{k}}\rangle^{(2)}}{dt} = \frac{18\pi M}{\hbar^3}\frac{\mathrm{Re}(g)^2}{V^2}\sum_{\mathbf{Q},\mathbf{q}}\left(\frac{\mathbf{Q}}{2}-\mathbf{k}\right)^2\left(\frac{\mathbf{Q}}{2}-\mathbf{q}\right)^2\delta(k^2-q^2+\mathbf{k}\cdot\mathbf{Q}-\mathbf{q}\cdot\mathbf{Q})\\ \times[(1-\langle N_{\mathbf{Q}-\mathbf{k}}\rangle)(1-\langle N_{\mathbf{k}}\rangle)\langle N_{\mathbf{q}}\rangle\langle N_{\mathbf{Q}-\mathbf{q}}\rangle - \langle N_{\mathbf{Q}-\mathbf{k}}\rangle\langle N_{\mathbf{k}}\rangle(1-\langle N_{\mathbf{q}}\rangle)(1-\langle N_{\mathbf{Q}-\mathbf{q}}\rangle)].\end{aligned} \tag{26}$$

Equation (26) contains the terms describing elastic collision, making $\mathcal{I}_{\mathrm{coll}}[Vn_{\mathbf{k}}]/V = \mathcal{I}_{\mathrm{inel}}[Vn_{\mathbf{k}}]/V + \mathcal{I}_{\mathrm{el}}[Vn_{\mathbf{k}}]/V$, where $\mathcal{I}_{\mathrm{el}}$ is the elastic collision integral, in contrast to the inelastic contribution. Explicitly, the form is given by

$$\begin{aligned}\mathcal{I}_{\mathrm{el}}[Vn_{\mathbf{k}}]/V = \frac{288\pi^3\hbar\,\mathrm{Re}(v_p)^2V}{M}\int\frac{d^3q}{(2\pi)^3}\int\frac{d^3Q}{(2\pi)^3}\delta(k^2-q^2+\mathbf{k}\cdot\mathbf{Q}-\mathbf{q}\cdot\mathbf{Q})\left(\frac{\mathbf{Q}}{2}-\mathbf{k}\right)^2\left(\frac{\mathbf{Q}}{2}-\mathbf{q}\right)^2\\ \times[(1-n_{\mathbf{Q}-\mathbf{k}}V)(1-n_{\mathbf{k}}V)n_{\mathbf{q}}n_{\mathbf{Q}-\mathbf{q}} - n_{\mathbf{Q}-\mathbf{k}}n_{\mathbf{k}}(1-n_{\mathbf{q}}V)(1-n_{\mathbf{Q}-\mathbf{q}}V)].\end{aligned} \tag{27}$$

IV. RELAXATION TIME OF *p*-WAVE ELASTIC COLLISION

In the Introduction, we state that recent experimental systems exhibiting only p-wave elastic collisions struggle to rethermalize from a nonequilibrium state. This observation is crucial, as it allows us to safely disregard the elastic collision integral when analyzing IQBE in subsequent discussions. Before validating this statement, it is essential to distinguish between two key assumptions in this work: (1) the system's interaction is weak, and (2) the system can hardly rethermalize. The first assumption implies that the interaction effect can be treated as a perturbation, i.e., $\mathrm{Re}(v_p)k_F^3 \ll 1$, where k_F is the system's Fermi momentum (divided by $\hbar$). The second assumption means that the relaxation time of elastic collisions is significantly longer than other timescales in the system. It is worth noting that these two assumptions are not inherently related. This section will use typical experimental data to support both assumptions.

We focus on two experimental realizations mentioned in the Introduction: rovibrational ground state $^{40}\mathrm{K}\,^{87}\mathrm{Rb}$ and $^{23}\mathrm{Na}\,^{40}\mathrm{K}$ molecular gases. The real parts of their bare scattering volumes v_p have been determined to be $(118a_0)^3$ [36] and $(88a_0)^3$ [27], respectively. The Fermi momentum of a harmonically trapped system is defined by $k_F = (48N)^{1/6}\sqrt{M\bar{\omega}/\hbar}$ [37]. For a conservative estimate, we deliberately overestimate the typical number of particles N in experiments to be 10^5 and assume the geometric mean of the harmonic trap's angular frequency $\bar{\omega}$ to be approximately $2\pi \times 100$ Hz. Using these values, we calculate $\mathrm{Re}(v_p)k_F^3$ for both systems, yielding approximately 7.5×10^{-4} and 1.1×10^{-4}, respectively. These values are significantly less than 1, supporting the weak interaction assumption.

To estimate the relaxation time, we begin with a simple derivation. We define the p-wave scattering volume from the phase shift δ_p, related to the scattering matrix S by

$$S = e^{2i\delta_p} \approx 1 + 2i\delta_p. \tag{28}$$

The expansion is valid because we have already shown that the interaction is weak enough: the phase shift should also be small. The elastic cross section is then given by

$$\sigma_{\mathrm{el}} = \frac{3\pi}{k^2}|1 - S|^2 \approx 12\pi[\mathrm{Re}(v_p)]^2(k_r)^4, \tag{29}$$

where k_r is the relative momentum between two scatters in a two-body collision. Defining the scattering energy $E = \hbar^2 k_r^2/M$, we can express σ_{el} as

$$\sigma_{\mathrm{el}}(E) = 12\pi[\mathrm{Re}(v_p)]^2\frac{M^2E^2}{\hbar^4}. \tag{30}$$

Assuming the trapped system is not in deep degeneracy, we can approximate the phase-space density of the cloud with a simple Gaussian distribution:

$$f(\mathbf{k}, \mathbf{r}) = z\,\exp\left(-\frac{\hbar^2k^2}{2Mk_BT}\right)\exp\left(-\frac{M\sum_i \omega_i^2 r_i^2}{2k_BT}\right), \tag{31}$$

where i represents x, y, and z directions of the harmonic trap. The fugacity $z = T_F^3/(6T^3)$, with $T_F = \hbar^2k_F^2/2M$, is determined by the normalization condition

$$N = \int \frac{d^3k}{(2\pi)^3}d^3r\, f(\mathbf{k}, \mathbf{r}; z). \tag{32}$$

Integrating the real-space dependence in f, we obtain the momentum distribution

$$f(\mathbf{k}) = z\left(\frac{2\pi k_BT}{M\omega^2}\right)^{3/2}\exp\left(-\frac{\hbar^2k^2}{2Mk_BT}\right). \tag{33}$$

For two colliding particles with momenta $\mathbf{k}_1$ and $\mathbf{k}_2$, the distribution is

$$f(\mathbf{k}_1)f(\mathbf{k}_2) = f(\mathbf{k}_r)f(\mathbf{k}_R), \tag{34}$$

where $\mathbf{k}_r = (\mathbf{k}_1 - \mathbf{k}_2)/2$ and $\mathbf{k}_R = \mathbf{k}_1 + \mathbf{k}_2$ are relative and center-of-mass momenta. Changing the argument of $f(\mathbf{k}_r)$ to E,

$$f(\mathbf{k}_r) = f(E) = z\left(\frac{2\pi k_BT}{M\omega^2}\right)^{3/2}\exp\left(-\frac{E}{k_BT}\right). \tag{35}$$

We then calculate

$$\begin{aligned}\langle\sigma_{\mathrm{el}}v_r\rangle &= \frac{1}{N}\int\frac{d^3k_r}{(2\pi)^3}f(E)\sigma_{\mathrm{el}}(E)v_r(E)\\ &= 1152\sqrt{2\pi}M^{3/2}[\mathrm{Re}(v_p)]^2(k_BT)^{5/2}/\hbar^4,\end{aligned} \tag{36}$$

where v_r is the relative speed of colliding particles, defined by $Mv_r^2/4 = E$. From Eq. (31), we obtain the *in situ* average density:

$$\begin{aligned}f(\mathbf{r}) &= \int\frac{d^3k}{(2\pi)^3}f(\mathbf{k}, \mathbf{r}),\\ \langle f(\mathbf{r})\rangle &= \frac{\int d^3r\, f(\mathbf{r})^2}{\int d^3r\, f(\mathbf{r})} = \frac{N}{8\pi^{3/2}}\bar{\omega}^3\left(\frac{k_BT}{M}\right)^{-3/2}.\end{aligned} \tag{37}$$

Combining Eqs. (36) and (37), we derive the timescale for one elastic collision event:

$$t_{\mathrm{el}} = \frac{1}{\langle\sigma_{\mathrm{el}}v_r\rangle\langle f(\mathbf{r})\rangle} = \frac{2^{19/6}\pi}{3^{4/3}N^{1/3}\left[\mathrm{Re}(v_p)k_F^3\right]^2(T/T_F)\bar{\omega}}. \tag{38}$$

The system's relaxation time should be αt_{el}, where α is typically larger than 1, indicating that each particle should collide more than once on average to reach equilibrium [13,38]. For our purposes, the exact value of α is less critical, as a sufficiently long t_{el} implies an even longer relaxation time.

Using the same parameters as in our previous discussion of $\mathrm{Re}(v_p)k_F^3$ and setting $T = T_F$, we calculate t_{el} for the two systems under consideration. The results are approximately 6 min for $^{40}\mathrm{K}\,^{87}\mathrm{Rb}$ and 5 h for $^{23}\mathrm{Na}\,^{40}\mathrm{K}$ molecular gases. Given that typical experimental durations are on the order of several seconds, these relaxation times for p-wave elastic collisions are significantly longer than other relevant timescales in these systems. This substantial difference in timescales supports our earlier assumption that the systems can hardly rethermalize through elastic collisions alone.

V. DYNAMICS OF HOMOGENEOUS SYSTEMS

In this section, we discuss solutions to the IQBE derived in Sec. III, focusing on homogeneous systems without external

potentials. As explained in Sec. IV, it is reasonable to ignore the elastic collision integral when modeling realistic cases. Therefore, we analyze the IQBE without elastic collisions. Then, we introduce effective temperatures to assess whether systems heat or cool after dissipation. We also compare our analytical approach with solutions obtained from the thermal ansatz, which assumes continuous thermalization during system dynamics.

For clarity, we employ dimensionless quantities throughout this section, denoted by a bar hat. Our chosen unit system is based on initial Fermi momentum $k_F(0) = [6\pi^2 N(0)/V]^{1/3}$, temperature $T_F(0) = \hbar^2 k_F(0)^2/2Mk_B$, and energy $E_F(0) = k_B T_F(0)$:

$$\begin{aligned} \text{momentum: } k &\to \bar{k} k_F(0), \\ \text{temperature: } T &\to \bar{T} T_F(0), \\ \text{time: } t &\to \bar{t}\hbar/E_F(0). \end{aligned}$$

It is important to note that we consistently use the *initial* particle number $N(0)$ rather than instantaneous particle number $N(t)$ as a reference for our units, hence the argument 0. This distinction becomes crucial when discussing systems using effective temperatures, where the effective Fermi temperature $T_F(t)$ varies with time. To avoid confusion, our unit system remains constant, i.e., generally, $\bar{T}_F(t) \neq 1$.

A. Mellin space analysis

Ignoring the elastic collision integral, the dimensionless form of IQBE (6) is

$$\frac{dN(\bar{k},\tau)}{d\tau} = -N(\bar{k},\tau)\int d\bar{q}(\bar{k}^2+\bar{q}^2)N(\bar{q},\tau), \tag{39}$$

where

$$\tau = -24\pi\,\mathrm{Im}(\bar{v}_p)\bar{t} = -12\pi\frac{\hbar k_F^5(0)}{M}\mathrm{Im}(v_p)t \tag{40}$$

is defined for convenience. $N(\bar{k},\tau)$ is defined to be

$$N(\bar{k},\tau) = \frac{4\pi\bar{k}^2 V n_{\bar{\mathbf{k}}}(\tau)}{(2\pi)^3},$$

which can be regarded as a one-dimensional (1D) projection of the momentum distribution. If we set the system to be thermalized initially, then the initial condition of $N(\bar{k},\tau)$ is

$$N(\bar{k},0) = \frac{3\bar{k}^2}{\exp\left(\frac{\bar{k}^2}{\bar{T}}\right)z^{-1}+1}, \quad z = -\mathrm{Li}_{\frac{3}{2}}^{-1}\left(\frac{-4}{3\sqrt{\pi}\bar{T}^{3/2}}\right), \tag{41}$$

where Li denotes the polylogarithm function and the index -1 signifies an inverse function. The Mellin transform of a function $g(x)$ is defined by

$$\mathcal{M}[g(x)](s) = \int_0^\infty dx\, x^{s-1} g(x). \tag{42}$$

We observe that Eq. (39) has a simpler form in Mellin space (of dimensionless momentum $\bar{k}$):

$$\begin{aligned} \frac{d\mathcal{M}[N(\bar{k},\tau)](s)}{d\tau} &= -\mathcal{M}[N(\bar{k},\tau)](s)\mathcal{M}[N(\bar{k},\tau)](3) \\ &\quad - \mathcal{M}[N(\bar{k},\tau)](s+2)\mathcal{M}[N(\bar{k},\tau)](1). \end{aligned} \tag{43}$$

Let us define $F_j = \mathcal{M}[N(\bar{k},\tau)](2j+1)$, the above equation becomes

$$\frac{dF_j(\tau)}{d\tau} = -F_j(\tau)F_1(\tau) - F_{j+1}(\tau)F_0(\tau). \tag{44}$$

Notably, the above equation's F_0 and F_1 are particularly important. It is easy to check that they represent the normalized total number of particles $N(\tau)/N(0)$ and total energy $N(\tau)\bar{E}(\tau)/N(0)$, respectively. Combining the definition of F_j and Eq. (41), at $\tau = 0$, the initial conditions of F_j are given by

$$F_j(0) = -\frac{3}{2}\bar{T}^{\frac{3}{2}+j}\Gamma\left(\frac{3}{2}+j\right)\mathrm{Li}_{\frac{3}{2}+j}(-z). \tag{45}$$

1. High-initial-temperature exact solution

In the high-initial-temperature limit $z \to 0$, Eq. (44) can be analytically solved. First, it is easy to find two crucial properties of high-order derivatives of $F_j(\tau)$ using Eq. (44): (1) the nth-order derivative of F_j is expressible as a sum of products of $n+1$ F terms, and (2) for each term, the sum of the indices of F equals $j+n$. Summarized, the relationship is

$$\begin{aligned} \frac{d^n F_j}{d\tau^n} &= (-1)^n \sum_{\substack{\{s_1,s_2,\ldots,s_{n+1}\} \\ \sum_i s_i = j+n}} C[j;\{s_1,s_2,\ldots,s_{n+1}\}] \\ &\quad \times F_{s_1}F_{s_2}\ldots F_{s_{n+1}}. \end{aligned} \tag{46}$$

The index i varies from 1 to $n+1$, and $C[j;\{s_1,s_2,\ldots,s_{n+1}\}]$ denotes the count of terms corresponding to a set of indices s_i. Figuring a general form for $C[j;\{s_1,s_2,\ldots,s_{n+1}\}]$ is generally challenging. However, with the high-temperature limit, the difficulty can be avoided. We do further one order of derivative to Eq. (46):

$$\begin{aligned} \frac{d^{n+1}}{d\tau^{n+1}}F_j &= (-1)^n \sum_{\substack{\{s_1,s_2,\ldots,s_{n+1}\} \\ \sum_i s_i = j+n}} C[j;\{s_1,s_2,\ldots,s_{n+1}\}] \\ &\quad \times \frac{\frac{d}{d\tau}\left(F_{s_1}F_{s_2}\ldots F_{s_{n+1}}\right)}{F_{s_1}F_{s_2}\ldots F_{s_{n+1}}} F_{s_1}F_{s_2}\ldots F_{s_{n+1}}. \end{aligned} \tag{47}$$

Using the general expression of Eq. (44),

$$\frac{\frac{d}{d\tau}\left(F_{s_1}F_{s_2}\ldots F_{s_{n+1}}\right)}{F_{s_1}F_{s_2}\ldots F_{s_{n+1}}} = -\sum_{k=1}^{n+1}\sum_{r=\{0,1\}}\frac{F_r F_{s_k+1-r}}{F_{s_k}}. \tag{48}$$

At high-temperature regime $\bar{T} \gg 1$, using the property of polylogarithm functions [39]

$$-\mathrm{Li}_s(-z) \xrightarrow{z\to 0} z, \tag{49}$$

the fugacity in Eq. (41) reduces to

$$z \xrightarrow{\bar{T}\to\infty} -\frac{4}{3\sqrt{\pi}\bar{T}^{3/2}} = \frac{1}{\Gamma(5/2)\bar{T}^{3/2}}. \tag{50}$$

Then, the initial condition (45) has the asymptote

$$F_j(0) \xrightarrow{\bar{T}\to\infty} \frac{3\bar{T}^j}{2}\frac{\Gamma\left(\frac{3}{2}+j\right)}{\Gamma\left(\frac{5}{2}\right)}. \tag{51}$$

Substituting Eq. (51) into (48) and taking $\tau = 0$,

$$\left.\frac{\frac{d}{d\tau}\left(F_{s_1}F_{s_2}\dots F_{s_{n+1}}\right)}{F_{s_1}F_{s_2}\dots F_{s_{n+1}}}\right|_{\tau=0} = -\bar{T}\sum_{k=1}^{n+1}(3+s_k). \tag{52}$$

Substituting back to Eq. (47),

$$\left.\frac{d^{n+1}}{d\tau^{n+1}}F_j\right|_{\tau=0} = (-1)^n \sum_{\substack{\{s_1,s_2,\dots,s_{n+1}\}\\ \sum_i s_i = j+n}} C[j;\{s_1,s_2,\dots,s_{n+1}\}] \times \left(F_{s_1}F_{s_2}\dots F_{s_{n+1}}\right)\left[-\bar{T}\left(3(n+1)+\sum_{i=1}^{n+1}s_i\right)\right]. \tag{53}$$

Because of the constraint $\sum_i s_i = j+n$ on the outermost summation,

$$\left.\frac{d^{n+1}}{d\tau^{n+1}}F_j\right|_{\tau=0} = (-1)^n \sum_{\substack{\{s_1,s_2,\dots,s_{n+1}\}\\ \sum_i s_i = j+n}} C[j;\{s_1,s_2,\dots,s_{n+1}\}]\left(F_{s_1}F_{s_2}\dots F_{s_{n+1}}\right)\{-\bar{T}[3(n+1)+(n+j)]\} = -\bar{T}[3(n+1)+(n+j)]\left.\frac{d^n}{d\tau^n}F_j\right|_{\tau=0}. \tag{54}$$

The recursion relation can be explicitly solved as

$$\left.\frac{d^n}{d\tau^n}F_j\right|_{\tau=0} = F_j(0)(-\bar{T})^n\prod_{n'=1}^{n}(4n'-1+j) = F_j(0)4^n(-\bar{T})^n\left(\frac{3+j}{4}\right)_n, \tag{55}$$

where $(a)_x = \Gamma(a+x)/\Gamma(a)$ is the Pochhammer symbol. Then, we find that $F_j(\tau)$ can be identified as the generalized hypergeometric function ${}_1F_0$,

$$F_j(\tau) = \sum_{n=0}^{\infty}\frac{\tau^n}{n!}\left.\frac{d^n}{d\tau^n}F_j\right|_{\tau=0} = F_j(0)\sum_{n=0}^{\infty}\frac{(-4\bar{T}\tau)^n}{n!}\left(\frac{3+j}{4}\right)_n = F_j(0)\,{}_1F_0\left(\frac{3+j}{4};-4\bar{T}\tau\right). \tag{56}$$

In fact, ${}_1F_0$ is nothing but a simple function:

$$F_j(\tau) = \frac{F_j(0)}{(1+4\bar{T}\tau)^{3/4+j/4}}. \tag{57}$$

Especially, for particle-number dynamics $F_0(\tau) = N(\tau)/N(0)$,

$$\frac{N(\tau)}{N(0)} = \frac{1}{(1+4\bar{T}\tau)^{3/4}}. \tag{58}$$

Equation (58) reveals an unexpected characteristic of the system: contrary to conventional $\mathcal{N}$-body recombination theory [40], the dissipation dynamics here do not follow a typical "two-body" loss pattern. The governing equation for an $\mathcal{N}$-body loss is generally expressed as

$$\frac{d}{d\tau}\left(\frac{N(\tau)}{N(0)}\right) = -K_{\mathcal{N}}\left(\frac{N(\tau)}{N(0)}\right)^{\mathcal{N}}, \tag{59}$$

where $K_{\mathcal{N}}$ represents the constant $\mathcal{N}$-body recombination rate coefficient. The general solutions to Eq. (59) are straightforward:

$$\frac{N(\tau)}{N(0)} = \begin{cases}\exp(-K_1\tau) & \text{for } \mathcal{N}=1,\\ [1+(\mathcal{N}-1)K_{\mathcal{N}}\tau]^{-1/(\mathcal{N}-1)} & \text{for } \mathcal{N}>1.\end{cases} \tag{60}$$

By comparing Eqs. (58) and (60), we deduce that

$$\mathcal{N} = \tfrac{7}{3}, \tag{61}$$

indicating a "fractional-body" loss process.

In the high-initial-temperature limit, it is possible to perform the inverse Mellin transform to find the full dynamics of $N(\bar{k},\tau)$. Equation (57) with Mellin frequency s as the argument is expressed as

$$\mathcal{M}[N(\bar{k},\tau)](s) = \frac{2}{\sqrt{\pi}}\bar{T}^{(s-1)/2}(1+4\bar{T}\tau)^{-(5+s)/8}\Gamma(s/2+1). \tag{62}$$

We first note that

$$\mathcal{M}^{-1}[(1+4\bar{T}\tau)^{-(5+s)/8}](\bar{k}) = (1+4\bar{T}\tau)^{-3/4} \times \delta[\bar{k}-(1+4\bar{T}\tau)^{-1/8}]. \tag{63}$$

And from Eq. (41), we know that

$$N(\bar{k},0)\big|_{z\to 0} = \mathcal{M}^{-1}\left[\frac{2}{\sqrt{\leqslant\pi}}\bar{T}^{(s-1)/2}\Gamma(s/2+1)\right](\bar{k}) = \frac{4\bar{k}^2}{\sqrt{\pi}\bar{T}^{3/2}}\exp\left(\frac{\bar{k}^2}{\bar{T}}\right). \tag{64}$$

Inverse Mellin transform has a property to convert multiplication to convolution [41]:

$$\mathcal{M}^{-1}[f(s)g(s)] = \int_0^\infty \frac{dy}{y}\mathcal{M}^{-1}[f]\left(\frac{x}{y}\right)\mathcal{M}^{-1}[g](y). \tag{65}$$

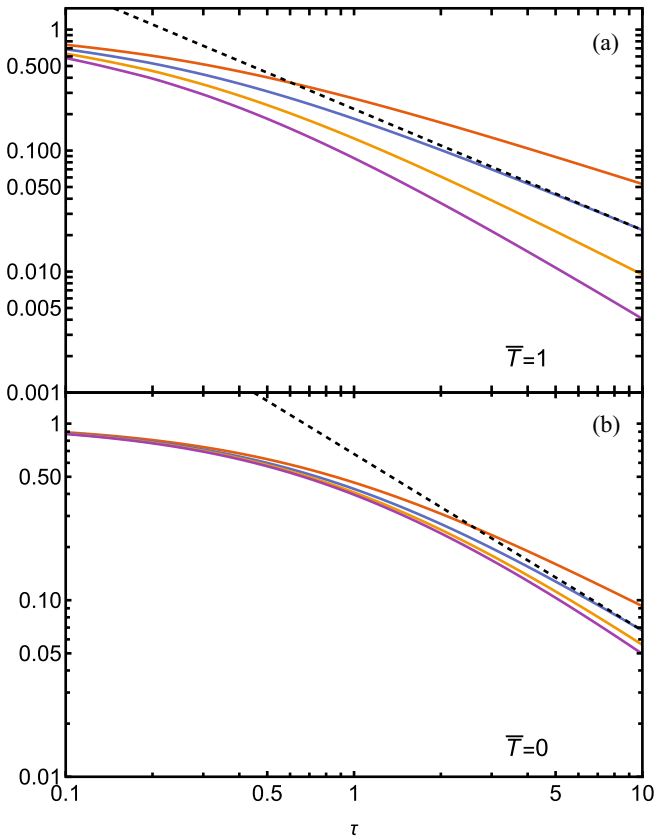

FIG. 1. Log-log plot of $F_0(\tau)/F_0(0)$ to $F_3(\tau)/F_0(0)$ from top to bottom for (a) $\bar{T}=1$ and (b) $\bar{T}=0$ showing the power-law tails of different F_n. The black dashed lines are $1/\tau$ eye guides demonstrating the power law of F_1 always has $x_1=1$ in a long time

Combining Eqs. (63), (64), and (65), we can perform the inverse transform of Eq. (62), which gives

$$N(\bar{k},\tau)=\frac{4\bar{k}^2}{\sqrt{\pi}\bar{T}^{3/2}(1+4\bar{T}\tau)^{3/8}}\exp\left(-(1+4\bar{T}\tau)^{1/4}\frac{\bar{k}^2}{\bar{T}}\right). \tag{66}$$

An important observation on Eq. (66) is that the momentum distribution is kept to be a Gaussian (the additional $\bar{k}^2$ comes from measurement $d^3\mathbf{k}$) for long-time dynamics, which motivates us to interpret it as an equilibrated profile. Indeed, we will see in Sec. (V B), Eq. (66) has the same expression as its corresponding thermal ansatz. In other words, the system can automatically be kept in equilibrium even without any elastic collision in the high-initial-temperature limit.

2. *Padé approximant method for arbitrary initial temperatures*

Generally, we conjecture all F_j decays in the power-law manner, i.e., $F_j \xrightarrow{\tau\to\infty} A_j\tau^{-x_j}$. The conjecture is correct for high-initial-temperature exact solutions (57). We also have numerical results in different temperatures verifying the conjecture shown in Fig. 1. Substituting this long-time ansatz into Eq. (44),

$$x_1=1 \text{ and } x_{j+1}-x_j=1-x_0, \tag{67}$$

$$x_jA_j=A_jA_1+A_{j+1}A_0. \tag{68}$$

From Eq. (67), one sees that

$$x_j=1+(j-1)(1-x_0) \tag{69}$$

is an arithmetic sequence with a common difference depending on x_0. Particularly, no matter the value of x_0, x_1 is always exactly 1, which, again, has been verified by numerical results in Fig. 1. This inspires us to construct approximation starting from F_1. A suitable functional form for F_1 is the Padé approximant $[m/n]_{F_1}(\tau)$, which is defined as

$$[m/n]_{F_1}(\tau)=\frac{\sum_{j=0}^{m}a_j\tau^j}{1+\sum_{k=0}^{n}b_k\tau^k},$$
$$\text{satisfying } \frac{d^j}{d\tau^j}[m/n]_{F_1}(\tau)=\frac{d^j}{d\tau^j}F_l(\tau)$$
$$(j=0,1,\ldots,n+m), \tag{70}$$

since if $n=m+1$, $\lim_{\tau\to\infty}[m/n]_{F_1}(\tau)\propto 1/\tau$. We expect in the limit $n=m+1\to\infty$, Eq. (70) can reproduce F_1 in an exact form. However, due to the difficulty of counting $C[j;\{s_1,s_2,\ldots,s_{n+1}\}]$, practically we cannot construct Padé approximant at a very high order.

The simplest construction is $[0/1]_{F_1}$, which only requires the information of $F_1(0)$ and $\frac{d}{d\tau}F_1(0)$. The latter can be directly read from Eq. (44), which is

$$\frac{d}{d\tau}F_1(0)=-[F_1(0)]^2-F_2(0). \tag{71}$$

Because $1/(1-x)=1+x+O(x^2)$, one can directly write the $[0/1]_{F_1}$ to be

$$F_1\simeq[0/1]_{F_1}=\frac{F_1(0)}{1+\left[F_1(0)+\dfrac{F_2(0)}{F_1(0)}\right]\tau}. \tag{72}$$

One may suspect that Eq. (72) is not accurate enough, especially for a short time, since it is the lowest-order approximation. However, as shown in Fig. 2, higher-order Padé approximants do not improve much. Therefore, we can believe Eq. (72) is a very reliable approximation of $F_1(\tau)$, and in the following discussion we will regard $F_1=[0/1]_{F_1}$. For $j=0$, Eq. (44) reduces to

$$\frac{dF_0(\tau)}{d\tau}=-2F_0(\tau)F_1(\tau), \tag{73}$$

thus we immediately obtain $F_0(\tau)$ when we know $F_1(\tau)$. Substituting Eq. (72) into (73),

$$\frac{N(\tau)}{N(0)}=F_0(\tau)=\left(1+\left[F_1(0)+\frac{F_2(0)}{F_1(0)}\right]\tau\right)^{\frac{-2F_1^2(0)}{F_1^2(0)+F_2(0)}}. \tag{74}$$

Again, by comparing Eqs. (74) and (60), we can extract $\mathcal{N}$ for this general situation:

$$\mathcal{N}=\frac{3}{2}+\frac{F_2(0)}{2F_1(0)^2}. \tag{75}$$

In the high-initial-temperature limit [i.e., Eq. (51)], as we expect, Eq. (75) has asymptotic value $\mathcal{N}=\frac{7}{3}$, which is consistent with the exact solution (61) solved above. Furthermore, one can also check that Eq. (74) recovers Eq. (58)

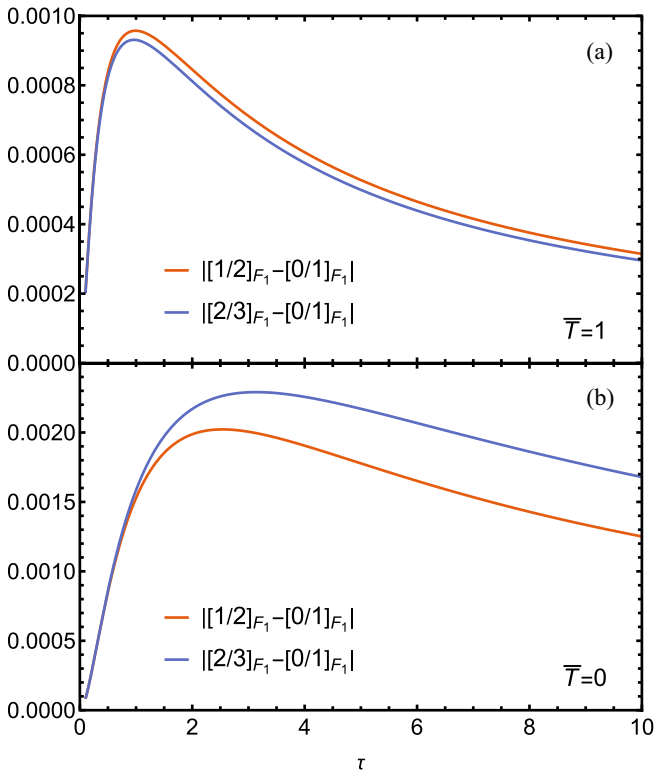

FIG. 2. Two examples demonstrating how accurate lowest-order Padé approximant is. (a) $\bar{T} = 1$. The expressions used for three approximants are $[0/1]_{F_1} = \frac{1.6967}{1+4.3677\tau}$, $[1/2]_{F_1} = \frac{1.6967+1.0153\tau}{1+4.9661\tau+2.6396\tau^2}$, and $[2/3]_{F_1} = \frac{1.6967-165.80\tau-107.40\tau^2}{1-93.352\tau-490.09\tau^2-279.03\tau^3}$. (b) $\bar{T} = 0$. The expressions used for three approximants are $[0/1]_{F_1} = \frac{0.6}{1+1.3143\tau}$, $[1/2]_{F_1} = \frac{0.6+0.19325\tau}{1+1.6364\tau+0.44144\tau^2}$, and $[2/3]_{F_1} = \frac{0.6+0.54310\tau+0.067246\tau^2}{1+2.2195\tau+1.3199\tau^2+0.15788\tau^3}$.

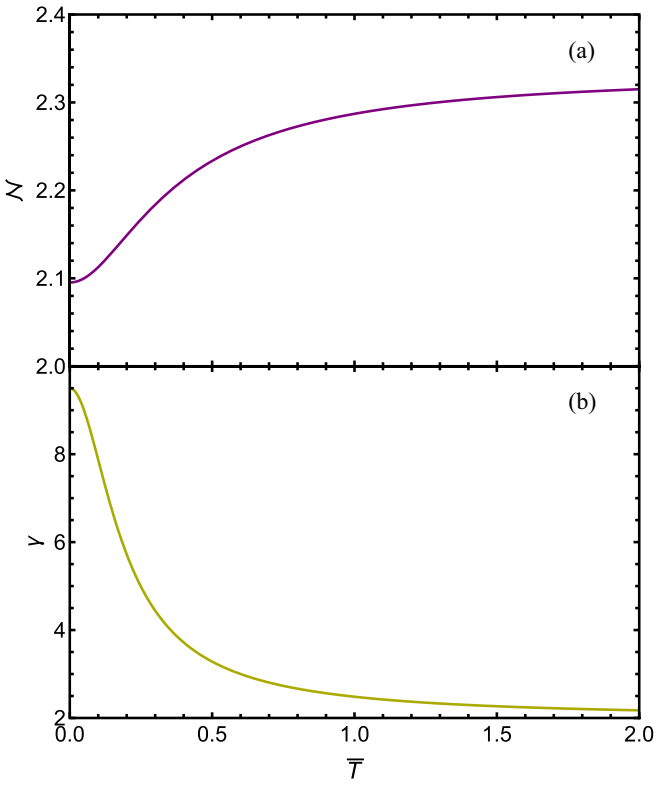

FIG. 3. Initial-temperature dependence of (a) $\mathcal{N}$ in Eq. (75) and (b) γ in Eq. (86).

exactly. We can also extract the asymptotic value for the zero-initial-temperature value as well. The asymptote of the polylogarithm function at the zero-temperature limit $z \to \infty$ is given by [39]

$$-\mathrm{Li}_s(-z) \xrightarrow{z\to+\infty} \frac{\ln(z)^s}{\Gamma(s+1)}. \tag{76}$$

Correspondingly,

$$-\mathrm{Li}_{s_1}\left[\mathrm{Li}_{s_2}^{-1}(-x)\right] \xrightarrow{x\to+\infty} \frac{[\Gamma(1+s_2)x]^{s_1/s_2}}{\Gamma(1+s_1)}, \tag{77}$$

$$F_j(0) \xrightarrow{\bar{T}\to 0} \frac{3}{3+2j}. \tag{78}$$

Hence,

$$\mathcal{N} \xrightarrow{\bar{T}\to 0} \frac{44}{21}, \tag{79}$$

which is still slightly larger than 2. As shown in Fig. 3(a), the two limits, Eqs. (61) and (79), are smoothly connected by a monotonically decreasing $\mathcal{N}$ with lowering temperatures. Consequently, the two-body dissipation dynamics in homogeneous single-component Fermi gases over all the temperatures cannot be described by conventional two-body decay where $\mathcal{N} = 2$.

Obtaining the full description of the momentum distribution dynamics is almost impossible for this arbitrary temperature scenario. The reason is that the inverse Mellin transform is generally too hard to perform. Below, we only show the infinite-time limit of momentum distribution dynamics. Practically, this is not a very relevant regime to experimental observation since, after a long time, the total number of particles left in the system will be too few to measure. However, this is still interesting from a pure theoretical aspect because long-term behavior tells whether the system can deviate from equilibrium.

According to Padé approximant (72) and its consequence (74), we can explicitly express

$$x_0 = \frac{2F_1^2(0)}{F_1^2(0)+F_2(0)}. \tag{80}$$

A_0 and A_1, the coefficient of decay power law in the long-time limit

$$A_0 = \left[F_1(0) + \frac{F_2(0)}{F_1(0)}\right]^{\frac{-2F_1^2(0)}{F_1^2(0)+F_2(0)}}, \quad A_1 = \frac{F_1(0)^2}{F_1(0)^2+F_2(0)}. \tag{81}$$

Equation (68) provides a recursion relation of A_j, thus we can express a general A_j with A_0 and A_1:

$$A_j = (x_0 - A_1)\left(\frac{A_0}{1-x_0}\right)^{1-j}\left(\frac{A_1-1}{x_0-1}\right)_{j-1}. \tag{82}$$

With Eqs. (69) and (82), we obtain the long-time asymptote of $F_j(\tau)$, or the Mellin transform of $N(\bar{k},\tau)|_{\tau\to\infty}$:

$$\mathcal{M}[N(\bar{k},\tau)](s)\big|_{\tau\to\infty} = (x_0-A_1)\left(\frac{A_0}{1-x_0}\right)^{\frac{3}{2}-\frac{s}{2}} \times \left(\frac{A_1-1}{x_0-1}\right)_{\frac{s}{2}-\frac{3}{2}} \tau^{-\frac{1}{2}[(1-x_0)s+3x_0-1]}, \tag{83}$$

as we note that

$$\mathcal{M}\big[\exp(-c_1k^2)k^{c_2}\big](s) = \frac{1}{2}c_1^{-\frac{s}{2}-\frac{c_2}{2}}\Gamma\left(\frac{s}{2}+\frac{c_2}{s}\right), \tag{84}$$

the inverse Mellin transform of Eq. (83) can be obtained as

$$N(\bar{k},\tau)\big|_{\tau\to\infty} = \frac{2A_0^2(x_0-A_1)}{(x_0-1)^2\Gamma\left(\frac{A_1-1}{x_0-1}\right)}\tau^{1-2x_0} \times \left(\sqrt{\frac{A_0}{1-x_0}\tau^{\frac{1}{2}-\frac{x_0}{2}}}\right)^{\frac{2(1+A_1-2x_0)}{x_0-1}} \times \exp\left(-\frac{A_0\tau^{1-x_0}}{1-x_0}\bar{k}^2\right)\bar{k}^\gamma, \tag{85}$$

where

$$\gamma = \frac{2(A_1-1)}{x_0-1} - 3. \tag{86}$$

First, it can be checked that Eq. (66) is consistent with Eq. (85) in the same limit, i.e., $\gamma = 2$. However, γ will no longer be 2 for a lower initial temperature, making the profile clearly of a nonequilibrium shape. For example, using Eq. (78), we find in the zero-initial-temperature limit, $\gamma = \frac{19}{2}$. Figure 3(b) shows the general calculation result of γ. Together with the conclusion we made previously in Sec. V A 1, the complete picture of the system's dissipation dynamics is as follows: with a high enough initial temperature, the system can be kept under equilibrium without elastic collision, while for lower initial temperatures, generally the two-body loss drives system away from being thermalized.

B. Effective temperatures and thermal ansatz

1. Dynamics of effective temperatures

Two-body dissipation is a crucial experimental consideration due to its heating effect on systems, which poses a significant obstacle to cooling processes [42,43]. This phenomenon, known as "antievaporation," was originally studied in the context of harmonically trapped systems. The conventional explanation for this heating mechanism is as follows: the center of the harmonic trap, being much denser than the periphery, experiences a higher rate of particle loss. Since particles in this region possess lower potential energy compared to those in other areas, their loss leads to an increase in the average energy per particle, consequently raising the system's temperature.

Our investigation aims to determine whether a similar phenomenon occurs in homogeneous systems. However, since dissipative dynamics generally drive systems out of equilibrium, we must first establish appropriate effective temperatures. We define these by hypothetically thermalizing the systems for measurement purposes. Thus, a system's effective temperature $T(t)$ is defined as the temperature of a thermalized system with identical particle number and total energy. Mathematically, we describe this corresponding thermalized system using a thermal ansatz:

$$N^{\rm th}(\bar{k},\tau) \equiv F_0(\tau)N^*(\bar{k},\tau), \tag{87}$$

where $N^*(\bar{k},\tau)$ is the normalized thermal momentum distribution:

$$d\bar{k}N^*(\bar{k},\tau) \equiv d\left(\frac{\bar{k}}{\bar{k}_F(\tau)}\right)\frac{3[\bar{k}/\bar{k}_F(\tau)]^2}{\exp\left[\frac{[\bar{k}/\bar{k}_F(\tau)]^2}{\bar{T}(\tau)/\bar{T}_F(\tau)}\right]z(\tau)^{-1}+1},$$
$$z(\tau) \equiv -\mathrm{Li}_{3/2}^{-1}\left(-\frac{4\bar{T}_F(\tau)^{3/2}}{3\sqrt{\pi}\bar{T}(\tau)^{3/2}}\right). \tag{88}$$

This expression is constructed by replacing all k_F and T_F at $\tau = 0$ with dynamic variables. The effective Fermi momentum $k_F(\tau)$ and effective Fermi temperature $T_F(\tau)$ are defined as

$$F_0(\tau) = \bar{k}_F(\tau)^3 = \bar{T}_F(\tau)^{3/2}. \tag{89}$$

Equation (89) ensures that the thermal system maintains the same particle number as the nonequilibrium profile. The total energy for this thermal ansatz is given by

$$E^{\rm th}(\tau) = \int d\bar{k}\,\bar{k}^2N^{\rm th}(\bar{k},\tau) = -\frac{9\sqrt{\pi}\bar{T}(\tau)^{5/2}}{8}\mathrm{Li}_{5/2}\left[\mathrm{Li}_{3/2}^{-1}\left(-\frac{4F_0(\tau)}{3\sqrt{\pi}\bar{T}(\tau)^{3/2}}\right)\right]. \tag{90}$$

We then implicitly determine $\bar{T}(\tau)$ by solving

$$F_1(\tau) = E^{\rm th}(\tau). \tag{91}$$

Figure 4 illustrates the dynamics of effective temperatures for four different initial temperatures. To assess whether the system is "cooled" or "heated," we employ two distinct criteria: one examines changes in the physical effective temperature $\bar{T}(\tau) = T(\tau)/T_F(0)$, while the other considers changes in the reduced effective temperature $\bar{T}(\tau)/\bar{T}_F(\tau) = T(\tau)/T_F(\tau)$. In Fig. 4(a), based on the first criterion, we observe that the physical effective temperature decreases at high initial temperatures. This can be attributed to the momentum dependence in the inelastic collision integral (22): particles with higher momenta are more likely to undergo inelastic collisions. Consequently, the chemical reaction in the system exhibits momentum selectivity, preferentially removing higher-energy particles and thus cooling the system. Conversely, at sufficiently low temperatures, inelastic collisions have the opposite effect, increasing the physical effective temperature as any perturbation to the Fermi sea generates excitations. Examining the reduced effective temperature in Fig. 4(b) reveals that, regardless of the initial temperature, inelastic collisions consistently drive the system away from quantum degeneracy.

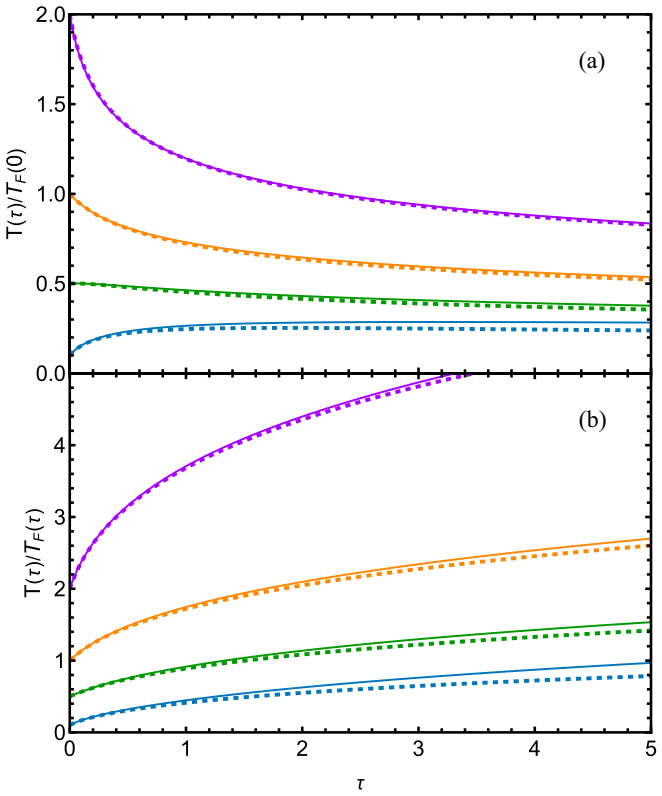

FIG. 4. Dynamics of effective temperatures for systems with initial temperatures $\bar{T}(0) = 2,\ 1,\ 0.5$, and 0.1 from above to below. Solid lines denote effective temperatures extracted from general nonequilibrium solutions of IQBE, i.e., Eqs. (74) and (72). The dotted lines are the results of solving IQBE by assuming that the thermal ansatz always applies. (a) The dynamics of physical effective temperature $\bar{T}(\tau) = T(\tau)/T_F(0)$. (b) The dynamics of reduced effective temperature $T(\tau)/T_F(\tau)$.

2. IQBE solution by assuming thermal ansatz

The thermal ansatz serves a dual purpose: it not only allows us to examine changes in effective temperatures but also enables us to assess the deviation of dissipation dynamics from the equilibrium limit. In this context, the equilibrium limit refers to dynamics where the system is assumed to thermalize instantaneously, such that $N(\bar{k},\tau) = N^{\rm th}(\bar{k},\tau)$ at every moment. Physically, this limit is equivalent to solving the IQBE with the elastic collision integral reintroduced under the constraint that elastic collisions occur on a much shorter timescale than inelastic collisions.

As discussed in Sec. IV, realistic scenarios often present the opposite situation. Consequently, our analysis in Sec. V A focuses on the IQBE while disregarding the elastic collision integral. However, if one were to retain the elastic collision integral, it is reasonable to expect that the exact solution would fall between the solution presented in Sec. V A and that obtained from the instant thermalization assumption. Thus, the following analysis also provides an upper bound for potential interaction effects within the system.

In the thermal ansatz, Eqs. (87) and (88), we need to determine two unknown quantities: $F_0(\tau)$ and $\bar{T}(\tau)$. For F_0, the equation of motion is straightforward:

$$\frac{dF_0(\tau)}{d\tau} = \int d\bar{k}\frac{d}{d\tau}N^{\rm th}(\bar{k},\tau) = \int d\bar{k}\,d\bar{q}(\bar{k}^2+\bar{q}^2)N^{\rm th}(\bar{q},\tau)N^{\rm th}(\bar{k},\tau) = -F_0^2 I_0, \tag{92}$$

where we utilize Eq. (39) in the second line. I_0 is explicitly expressed as

$$I_0(\tau) = -\frac{9\sqrt{\pi}\bar{T}(\tau)^{5/2}}{4F_0(\tau)}\mathrm{Li}_{5/2}\left[\mathrm{Li}^{-1}_{3/2}\left(-\frac{4F_0(\tau)}{3\sqrt{\pi}\bar{T}(\tau)^{3/2}}\right)\right]. \tag{93}$$

The equation of motion for $\bar{T}(\tau)$ is derived from the temporal change of energy per particle $\mathcal{E}^{\rm th} = E^{\rm th}/F_0$:

$$\frac{d\mathcal{E}^{\rm th}}{d\tau} = \frac{\partial\mathcal{E}^{\rm th}}{\partial F_0}\frac{dF_0}{d\tau} + \frac{\partial\mathcal{E}^{\rm th}}{\partial\bar{T}}\frac{d\bar{T}}{d\tau} = -F_0^2 I_0\frac{\partial\mathcal{E}^{\rm th}}{\partial F_0} + \frac{\partial\mathcal{E}^{\rm th}}{\partial\bar{T}}\frac{d\bar{T}}{d\tau}, \tag{94}$$

$$\frac{d\mathcal{E}^{\rm th}}{d\tau} = \int d\bar{k}\,\bar{k}^2\frac{dN^*(\bar{k},\tau)}{d\tau} = -F_0 I_2 + \mathcal{E}^{\rm th}F_0^2 I_0, \tag{95}$$

where

$$I_2(\tau) = \int d\bar{k}\,d\bar{q}\,\bar{k}^2(\bar{k}^2+\bar{q}^2)N^*(\bar{q},\tau)N^*(\bar{k},\tau) = \frac{81\pi\bar{T}(\tau)^5\mathrm{Li}^2_{5/2}\left[\mathrm{Li}^{-1}_{3/2}\left(-\frac{4F_0(\tau)}{3\sqrt{\pi}\bar{T}(\tau)^{3/2}}\right)\right]}{64F_0(\tau^2)} - \frac{45\sqrt{\pi}\bar{T}(\tau)^{7/2}\mathrm{Li}_{7/2}\left[\mathrm{Li}^{-1}_{3/2}\left(-\frac{4F_0(\tau)}{3\sqrt{\pi}\bar{T}(\tau)^{3/2}}\right)\right]}{16F_0(\tau)}. \tag{96}$$

From Eqs. (94) and (95), we derive

$$\frac{d\bar{T}(\tau)}{d\tau} = \frac{(d\mathcal{E}^{\rm th}/dF_0)F_0^2 I_0 + \mathcal{E}^{\rm th}F_0 I_0 - F_0 I_2}{(d\mathcal{E}^{\rm th}/d\bar{T})}. \tag{97}$$

The explicit forms of $d\mathcal{E}^{\rm th}/dF_0$ and $d\mathcal{E}^{\rm th}/d\bar{T}$ are obtained from Eq. (90):

$$\frac{d\mathcal{E}^{\rm th}}{dF_0} = -\frac{2}{\sqrt{\pi}\sqrt{\bar{T}}\mathrm{Li}_{1/2}\left[\mathrm{Li}^{-1}_{3/2}\left(-\frac{4F_0(\tau)}{3\sqrt{\pi}\bar{T}(\tau)^{3/2}}\right)\right]} + \frac{9\sqrt{\pi}\bar{T}^{5/2}\mathrm{Li}_{5/2}\left[\mathrm{Li}^{-1}_{3/2}\left(-\frac{4F_0(\tau)}{3\sqrt{\pi}\bar{T}(\tau)^{3/2}}\right)\right]}{8F_0^2}, \tag{98}$$

$$\frac{d\mathcal{E}^{\rm th}}{d\bar{T}} = \frac{3F_0}{\sqrt{\pi}\bar{T}^{3/2}\mathrm{Li}_{1/2}\left[\mathrm{Li}^{-1}_{3/2}\left(-\frac{4F_0(\tau)}{3\sqrt{\pi}\bar{T}(\tau)^{3/2}}\right)\right]} - \frac{45\sqrt{\pi}\bar{T}^{3/2}\mathrm{Li}_{5/2}\left[\mathrm{Li}^{-1}_{3/2}\left(-\frac{4F_0(\tau)}{3\sqrt{\pi}\bar{T}(\tau)^{3/2}}\right)\right]}{16F_0}. \tag{99}$$

The coupled Eqs. (92) and (97) generally require numerical solutions. However, in the high-initial-temperature limit, following Eq. (49), they simplify to

$$dF_0(\tau)/d\tau = -3\bar{T}(\tau)F_0(\tau)^2,\qquad d\bar{T}(\tau)/d\tau = -F_0(\tau)\bar{T}(\tau)^2. \tag{100}$$

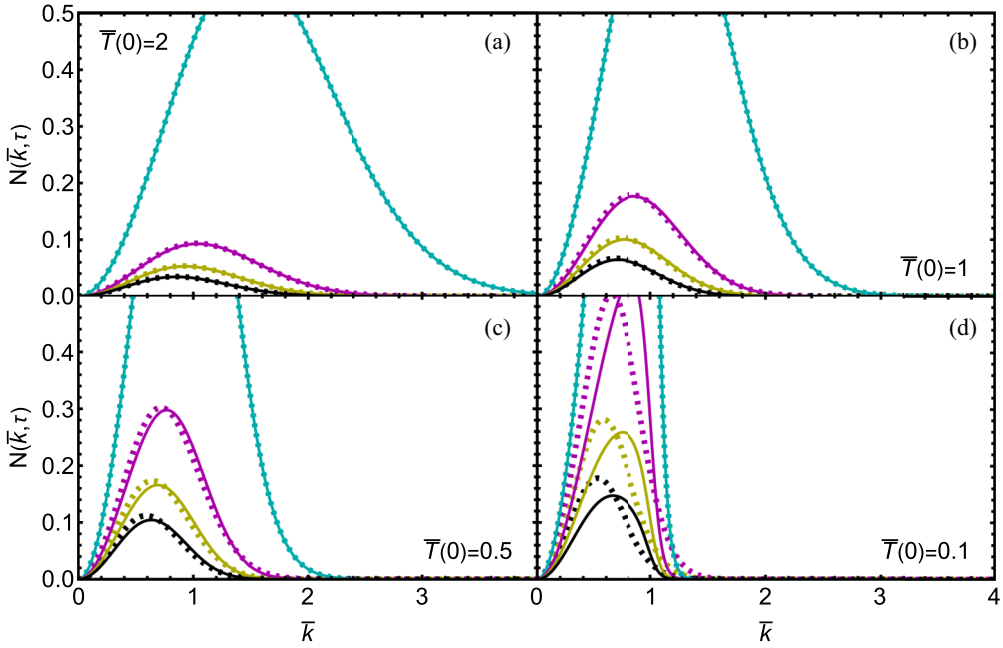

FIG. 5. Comparison between thermalized momentum distribution (dotted lines) solved from the thermal ansatz and nonequilibrium momentum distribution (solid lines) solved from Eq. (39) at different time shots $\tau = 0, 2, 5$, and 10 denoted by cyan, magenta, yellow, and black colors, respectively.

Solving this set of equations yields

$$F_0(\tau) = \frac{1}{[1+4\bar{T}(0)\tau]^{3/4}}, \quad \bar{T}(\tau) = \frac{\bar{T}(0)}{[1+4\bar{T}(0)\tau]^{1/4}}. \tag{101}$$

Notably, $F_0(\tau)$ in Eq. (101) is identical to Eq. (58). Moreover, substituting Eq. (101) into Eqs. (87) and (88) recovers Eq. (66), corroborating our conclusion in Sec. V A 1 that elastic collisions play no role in systems with high initial temperatures. We can also analytically study $T(\tau)/T_F(\tau)$ using Eq. (89):

$$\frac{T(\tau)}{T_F(\tau)} = \frac{T(0)}{T_F(0)}\left[1+\frac{4T(0)\tau}{T_F(0)}\right]^{\frac{1}{4}}, \tag{102}$$

which increases monotonically, consistent with our findings in Sec. V B 1.

For general situations, we numerically solve Eqs. (92) and (97). Figure 4 compares $\bar{T}(\tau)$ and $T(\tau)/T_F(\tau)$ with the general nonequilibrium solution of the IQBE. Surprisingly, except for systems initially in deep quantum degeneracy [$T(0)/T_F(0) = 0.1$]), all cases show remarkable similarity. This demonstrates that for initial temperatures not excessively low, systems without elastic collisions remain close to equilibrium for reasonable periods. Figure 5 provides a more intuitive comparison of $N(\bar{k}, \tau)$ between nonequilibrium solutions calculated using Eq. (39) and results from the thermal ansatz.

VI. DYNAMICS OF HARMONICALLY TRAPPED SYSTEMS

This section examines systems confined in a harmonic trap, where the dynamics are governed by Eq. (5). Unlike Eq. (6), which can be reduced to a one-dimensional equation [Eq. (39)] due to the spherical symmetry of $n_{\mathbf{k}}$, Eq. (5) exhibits an irreducible six-dimensional spatial complexity. This complexity renders direct numerical solutions impractical.

As with homogeneous systems, we employ dimensionless quantities to simplify our notation. To facilitate the treatment of phase space as a unified whole, we introduce two distinct length scales for dimensionless representations: the inverse of the Fermi momentum $1/k_F^{\rm trap}$ and the Thomas-Fermi radius $R_F^{\rm trap}$. These are defined as follows: For one-dimensional systems (used in Sec. VI A),

$$\frac{1}{k_F^{\rm trap}} = \frac{1}{\sqrt{2N(0)}}\sqrt{\frac{\hbar}{M\omega}}, \quad R_F^{\rm trap} = \sqrt{2N(0)}\sqrt{\frac{\hbar}{M\omega}}. \tag{103}$$

For three-dimensional systems,

$$\frac{1}{k_F^{\rm trap}} = [48N(0)]^{-\frac{1}{6}}\sqrt{\frac{\hbar}{M\omega}}, \quad R_F^{\rm trap} = [48N(0)]^{\frac{1}{6}}\sqrt{\frac{\hbar}{M\omega}}. \tag{104}$$

In 1D systems, ω represents the angular frequency of the trap. For 3D cases, it denotes the geometric mean of angular frequencies in all three directions:

$$\omega = (\omega_x\omega_y\omega_z)^{1/3}. \tag{105}$$

Our notation for dimensionless quantities follows these conventions:

(i) Quantities in units of $1/k_F^{\rm trap}$ or its derivatives [such as $k_F^{\rm trap}$ (wave vector), $E_F^{\rm trap} = \frac{\hbar^2(k_F^{\rm trap})^2}{2M}$ (energy), $T_F^{\rm trap} = E_F^{\rm trap}/k_B$ (temperature)] are denoted with a "bar" (e.g., $\bar{k}$).

(ii) Quantities in units of $R_F^{\rm trap}$ or its derivatives are denoted with a "tilde" (e.g., $\tilde{r}$).

For anisotropic 3D systems ($\omega_x \neq \omega_y \neq \omega_z$), we introduce a modified position vector $\mathbf{x}$, related to the physical position

r by

$$\mathbf{x} = \left(\frac{\omega_x}{\omega} r_x, \frac{\omega_y}{\omega} r_y, \frac{\omega_z}{\omega} r_z\right). \tag{106}$$

This formulation provides a consistent framework for analyzing trapped systems across different dimensionalities and trap geometries.

A. Fast-flowing approximation

To address the computational challenges posed by the six-dimensional nature of the IQBE, we introduce the fast-flowing approximation (FFA). This approach assumes that the distribution function $f(\mathbf{k}, \mathbf{r}, t)$ maintains hyperspherical symmetry throughout the entire phase space, such that $f(\mathbf{k}, \mathbf{r}, t) \equiv f(R, t)$, where

$$R = \sqrt{\bar{k}^2 + \tilde{x}^2} = \sqrt{\sum_{i=x,y,z} \left(\bar{k}_i^2 + \omega_i^2 \tilde{r}_i^2/\omega^2\right)}. \tag{107}$$

We assume that at $t = 0$, the systems are prepared in thermalized states, which inherently possess hyperspherical symmetry:

$$f(\mathbf{k}, \mathbf{r}, 0) = f(R, 0) = \frac{48}{\exp\left(\frac{R^2}{\bar{T}}\right)(z^{\text{trap}})^{-1} + 1}, \tag{108}$$

where the fugacity in trapped systems is given by

$$z^{\text{trap}} = -\text{Li}_3^{-1}\left(-\frac{1}{6\bar{T}^3}\right). \tag{109}$$

The validity of this approximation for systems that have evolved over time can be justified by considering the disparate timescales involved in experimental setups. Harmonic trap dynamics typically operate on a much faster timescale than two-body relaxation processes. For instance, with an average trap frequency of $2\pi \times 100$ Hz, the associated timescale is approximately 1 ms. In contrast, the typical relaxation process unfolds over several seconds. This significant separation of timescales implies that the molecular cloud's dynamics are substantially faster than the relaxation reactions. Consequently, we can neglect inelastic collisions within short time intervals, allowing the system to reach a quasisteady state. It can be readily demonstrated that the steady-state phase-space distributions, obtained by solving

$$\left[\frac{\hbar \mathbf{k}}{M} \nabla_{\mathbf{r}} - \frac{\nabla_{\mathbf{r}} U_{\text{ext}} \cdot \nabla_{\mathbf{k}}}{\hbar}\right] f = 0 \tag{110}$$

indeed exhibit the hyperspherical symmetry $f(\mathbf{k}, \mathbf{r}, t) = f(R, t)$. This fast-flowing approximation provides a tractable approach to modeling the complex dynamics of trapped systems while capturing the essential physics of the problem.

1. Validating FFA with 1D analog

To validate the fast-flowing approximation (FFA), we initially applied it to a simplified one-dimensional version of the problem. The dimensionless form of the inelastic Boltzmann equation in this context is

$$\frac{df}{d(\omega t)} = \left[\tilde{x}\partial_{\bar{k}} - \bar{k}\partial_{\tilde{x}} - G \int \frac{d\bar{q}}{2\pi}(\bar{k}^2 + \bar{q}^2) f(\bar{q}, \tilde{x})\right] f(\bar{k}, \tilde{x}), \tag{111}$$

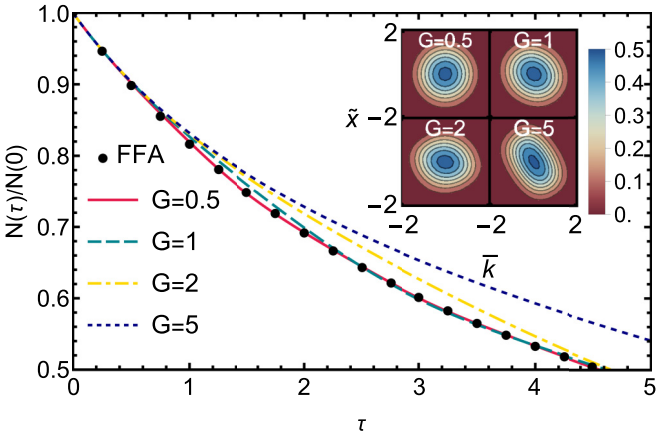

FIG. 6. Comparison between brute-force numerical solutions of Eq. (111) with different G and the result from Eq. (112). The initial temperature is set to be $\bar{T} = 1$ in 1D, i.e., $f(\bar{k}, \tilde{x}, 0) = [\exp(\bar{k}^2 + \tilde{x}^2)/(e-1) + 1]^{-1}$. Inset: phase-space density $f(\bar{k}, \tilde{x}, \tau)$ at $\tau = 5$.

where G represents the dimensionless reaction strength, with higher values indicating more rapid relaxation, it is important to note that Eq. (111) serves as an analog to the 3D problem we are focusing on and may not accurately describe a physical 1D or quasi-1D system. Within the FFA framework, this equation simplifies to

$$\frac{df(R)}{d\tau} = -\frac{1}{4\pi^2} \int_0^{2\pi} d\theta \int_0^{\infty} d\bar{q}(R^2 \cos^2\theta + \bar{q}^2) \times f(\sqrt{R^2 \sin^2\theta + \bar{q}^2}) f(R), \tag{112}$$

where $\tau = G\omega t$ and $R = \sqrt{\bar{k}^2 + \tilde{x}^2}$.

We performed numerical solutions of Eq. (111) for various G values and compared them with the predictions of Eq. (112), as shown in Fig. 2. The results demonstrate improved agreement for smaller G values, supporting the assumption that FFA is valid when the reaction rate is sufficiently slow. The inset of Fig. 6 provides an intuitive visualization of the phase-space density at $\tau = 5$ for different G values. This reinforces the assumption that f maintains spherical symmetry throughout the process, further validating the FFA approach. These findings provide a solid foundation for applying the fast-flowing approximation to more complex three-dimensional systems where direct numerical solutions are computationally prohibitive.

2. 3D IQBE under FFA

We now extend our analysis to realistic 3D cases. First, we express Eq. (5) in dimensionless form

$$\frac{df(\bar{\mathbf{k}}, \tilde{\mathbf{x}}, \bar{t})}{d\bar{t}} = \left[-\frac{\hbar\omega}{E_F^{\text{trap}}} \bar{\mathbf{k}} \cdot \nabla_{\tilde{\mathbf{x}}} + \frac{\hbar\omega}{E_F^{\text{trap}}} \tilde{\mathbf{x}} \cdot \nabla_{\bar{\mathbf{k}}}\right] f(\bar{\mathbf{k}}, \tilde{\mathbf{x}}, \bar{t}) + 24\pi \, \text{Im}(\bar{v}_p) \int \frac{d^3\bar{q}}{(2\pi)^3} \times (\bar{q}^2 + \bar{k}^2) f(\bar{\mathbf{k}}, \tilde{\mathbf{x}}, \bar{t}) f(\bar{\mathbf{q}}, \tilde{\mathbf{x}}, \bar{t}). \tag{113}$$

After nondimensionalization, the normalization of $f(\bar{\mathbf{k}}, \tilde{\mathbf{x}}, \bar{t})$ becomes

$$\int d^3\tilde{x}\frac{d^3\bar{k}}{(2\pi)^3}f(\bar{\mathbf{k}}, \tilde{\mathbf{x}}, \bar{t}) = \frac{N(t)}{48N(0)}. \tag{114}$$

This additional factor arises from $k_F^{\rm trap}R_F^{\rm trap} = (48N(0)\prod_{i=x,y,z}\omega_i/\omega)^{1/3}$. For numerical convenience, we redefine the dimensionless phase-space density as $\mathcal{F}(\bar{\mathbf{k}}, \tilde{\mathbf{x}}, \bar{t}) = 48f(\bar{\mathbf{k}}, \tilde{\mathbf{x}}, \bar{t})$. Equation (113) can then be rewritten as

$$\begin{aligned}\frac{d\mathcal{F}(\bar{\mathbf{k}}, \tilde{\mathbf{x}}, \tau^{\rm trap})}{d\tau^{\rm trap}} &= \left[\frac{2\hbar\omega}{\pi\,{\rm Im}(\bar{v}_p)E_F^{\rm trap}}\bar{\mathbf{k}}\cdot\nabla_{\tilde{\mathbf{x}}} - \frac{2\hbar\omega}{\pi\,{\rm Im}(\bar{v}_p)E_F^{\rm trap}}\tilde{\mathbf{x}}\cdot\nabla_{\bar{\mathbf{k}}}\right]\mathcal{F}(\bar{\mathbf{k}}, \tilde{\mathbf{x}}, \bar{t}) \\ &\quad - \int\frac{d^3\bar{q}}{(2\pi)^3}(\bar{q}^2+\bar{k}^2)\mathcal{F}(\bar{\mathbf{k}}, \tilde{\mathbf{x}}, \tau^{\rm trap})\mathcal{F}(\bar{\mathbf{q}}, \tilde{\mathbf{x}}, \tau^{\rm trap}),\end{aligned} \tag{115}$$

where $\tau^{\rm trap} = \frac{\pi}{2}{\rm Im}(\bar{v}_p)\bar{t} = -\frac{\pi\hbar[k_F^{\rm trap}(0)]^5}{4M}{\rm Im}(v_p)t$.

The FFA allows us to express $\mathcal{F}(\bar{\mathbf{k}}, \tilde{\mathbf{x}}, \tau^{\rm trap})$ solely in terms of the hyperradius $R = \sqrt{\bar{k}^2+\tilde{x}^2}$, i.e., $\mathcal{F}(\bar{\mathbf{k}}, \tilde{\mathbf{x}}, \tau^{\rm trap}) = \mathcal{F}(R, \tau^{\rm trap})$. Consequently,

$$\left[-\frac{2\hbar\omega\bar{\mathbf{k}}\cdot\nabla_{\tilde{\mathbf{x}}}}{\pi\,{\rm Im}(\bar{v}_p)E_F^{\rm trap}} + \frac{2\hbar\omega\tilde{\mathbf{x}}\cdot\nabla_{\bar{\mathbf{k}}}}{\pi\,{\rm Im}(\bar{v}_p)E_F^{\rm trap}}\right]\mathcal{F}(R, \bar{t}) = 0. \tag{116}$$

To convert other terms to hyperspherical coordinates, we employ the necessary integral measures in Eq. (115):

$$\begin{aligned}&\int d^3\tilde{x}\,d^3\bar{k}\frac{d\mathcal{F}(\bar{\mathbf{k}}, \tilde{\mathbf{x}}, \tau^{\rm trap})}{d\tau^{\rm trap}} \\ &= \int d\Omega^{(5)}\frac{d\mathcal{F}(R, \tau^{\rm trap})}{d\tau^{\rm trap}} \\ &= -\int d\Omega^{(5)}\int\frac{d^3\bar{q}}{(2\pi)^3}(\bar{q}^2+R^2h) \\ &\quad\times\mathcal{F}(R, \tau^{\rm trap})\mathcal{F}(\sqrt{\bar{q}^2+R^2(1-h)}, \tau^{\rm trap}),\end{aligned} \tag{117}$$

where $\Omega^{(5)}$ is the solid angle in five dimensions (5D) with the measure

$$d\Omega^{(5)} = \sin^4(\theta_1)\sin^3(\theta_2)\sin^2(\theta_3)\sin(\theta_4)d\theta_1 d\theta_2 d\theta_3 d\theta_4 d\phi \tag{118}$$

and h is a function of $\Omega^{(5)}$:

$$h[\Omega^{(5)}] = \cos^2\theta_1 + \sin^2\theta_1\cos^2\theta_2 + \sin^2\theta_1\sin^2\theta_2\cos^2\theta_3. \tag{119}$$

The ranges of polar angles θ_1 to θ_5 are 0 to π, and the range of azimuth angle ϕ is 0 to 2π. As $\int d\Omega^{(5)} = \pi^3$, Eq. (117) simplifies to

$$\begin{aligned}\frac{d\mathcal{F}(R, \tau^{\rm trap})}{d\tau^{\rm trap}} &= -\frac{2}{\pi^4}\int d\theta_1 d\theta_2 d\theta_3\sin^4\theta_1 d\,\sin^3\theta_2 d\,\sin^2\theta_3 \\ &\quad\times\int d\bar{q}\,\bar{q}^2(\bar{q}^2+R^2h)\mathcal{F}(R, \tau^{\rm trap}) \\ &\quad\times\mathcal{F}(\sqrt{\bar{q}^2+R^2(1-h)}, \tau^{\rm trap}).\end{aligned} \tag{120}$$

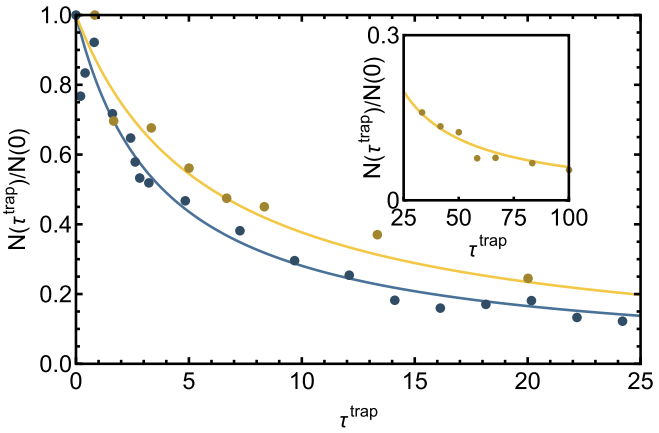

FIG. 7. Reproducing experimental data in Ref. [26] by numerically solving Eq. (120). Yellow and blue colors represent systems with initial temperatures $\bar{T} = 1.26$ and 0.48, respectively. Solid lines are our numerical results, and circle symbols are raw experimental data reported in Ref. [26].

Equation (120) represents the FFA of a 3D harmonically trapped system suitable for numerical analysis. To interpret results, we can use the following properties of $\mathcal{F}(R, \tau^{\rm trap})$ to obtain the normalized total number of particles and average energy per particle:

$$\frac{N(\tau^{\rm trap})}{N(0)} = \frac{1}{8}\int_0^\infty dR\,R^5\mathcal{F}(R, \tau^{\rm trap}), \tag{121}$$

$$\frac{E(\tau^{\rm trap})}{N(\tau^{\rm trap})} = \frac{1}{3}\frac{\int_0^\infty dR\,R^7\mathcal{F}(R, \tau^{\rm trap})}{\int_0^\infty dR\,R^5\mathcal{F}(R, \tau^{\rm trap})}. \tag{122}$$

Figure 7 demonstrates the application of this approach to reproduce experimental data from Ref. [26] by numerically solving Eq. (120). The results for systems with initial temperatures $\bar{T} = 1.26$ and 0.48 are shown, with solid lines representing our numerical results and circle symbols indicating raw experimental data from Ref. [26].

3. Comparison with experimental data

To demonstrate the predictive power of Eq. (120), we reproduce the experimental measurements reported in Ref. [26]. Using the raw data provided in Ref. [26], we analyze two decay measurement sets with initial reduced temperatures $\bar{T} = 1.26$ and 0.48. The imaginary part of the scattering volume is set to ${\rm Im}(v_p) = -(118a_0)^3$, consistent with previous studies [33,36].

Figure 7 presents a comparison between the dynamics predicted by Eq. (120) and the raw experimental data using the dimensionless unit system introduced in this section. Our theoretical calculations show excellent agreement with the experimental results, even over extended timescales. Specifically, we achieve good correspondence up to $\tau^{\rm trap} = 100$ for the $\bar{T} = 1.26$ sample and $\tau^{\rm trap} = 25$ for the $\bar{T} = 0.48$ sample. These dimensionless times translate to a physical duration of approximately 6 s, demonstrating the robustness of our approach in capturing long-term system behavior.

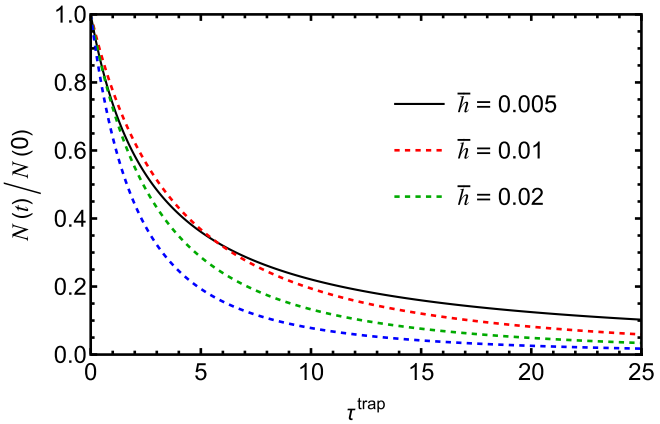

FIG. 8. Comparison between the fast-flowing approximation calculation at $\bar{T} = 0.1$ (solid line) and predictions from Ref. [33] (dashed lines) using different phenomenological heating rates $\bar{h}$.

It is worth mentioning that the IQBE approach is also applicable and convenient to be used for reproducing short-time dynamics and comparison with experimental loss rates (see Appendix B).

4. Comparison with theory explicitly considering antievaporation

Previous theories have studied the antievaporation process with the temperature increase strictly linearly. For instance, Ref. [33] introduced a phenomenological heating rate parameter h to account for linear temperature increase. To directly compare with these approaches, we examine the particle-number dynamics predicted by both methods. For a fair comparison, we rewrite the result from Ref. [33] in the dimensionless form

$$\frac{N(t)}{N(0)} = \frac{(1+\bar{h}\tau^{\mathrm{trap}}/\bar{T})^{3/2}}{1+\dfrac{\sqrt{2}\int \tilde{k}^2 f(\bar{\mathbf{k}},\tilde{\mathbf{r}},0)d^3r\,d\tilde{k}}{8\pi^{3/2}h\bar{T}}\left(\sqrt{1+\dfrac{\bar{h}\tau^{\mathrm{trap}}}{\bar{T}}}-1\right)}. \tag{123}$$

The dimensionless phenomenological heating rate $\bar{h}$ is defined as $\bar{h} = -\frac{4Mh}{\pi\hbar[k_F^{\mathrm{trap}}(0)]^5 T_F^{\mathrm{trap}}\mathrm{Im}(\upsilon_p)}$.

Figure 8 demonstrates the comparison at $\bar{T} = 0.1$. We plot our fast-flowing approximation result alongside predictions from Ref. [33] using three different phenomenological heating rates: $\bar{h} = 0.005$, 0.01, and 0.02. These values correspond to particle numbers $N \approx 46\,000$, 24 000, and 14 000, respectively, based on the experimental heating rate of approximately 20 nK/s reported in Ref. [33]. Regardless of how we tune the phenomenological parameter $\bar{h}$, the curves from Ref. [33] differ slightly from our predictions. This suggests that the temperature increase during the antievaporation deviates from a straight line.

Note that, in comparison, in our framework, heating emerges naturally from the underlying microscopic physics of inelastic collisions and trap geometry. Given a fixed (and independently measured) complex scattering volume, our model fully determines the system's evolution without additional free parameters.

B. Thermal ansatz

Equation (120) is significantly more complex than its homogeneous counterpart, for which we lack an analytical solution method. However, drawing on our experience with homogeneous systems, where the thermal ansatz effectively describes dynamics at high initial temperatures, we conjecture that a similar approach may provide a good approximation for trapped systems with high initial temperatures.

Following the procedure in Sec. V B 1, we introduce the thermal ansatz

$$\mathcal{F}^{\mathrm{th}}(R,\tau^{\mathrm{trap}}) \equiv F_0(\tau^{\mathrm{trap}})\mathcal{F}^*(R,\tau^{\mathrm{trap}}) \tag{124}$$

into Eq. (120), where F_0 represents $N(\tau^{\mathrm{trap}})/N(0)$ and

$$dR\mathcal{F}^*(R,\tau^{\mathrm{trap}}) \equiv \frac{dR}{F_0(\tau^{\mathrm{trap}})}\frac{48}{\exp\left(\frac{R^2}{\bar{T}(\tau^{\mathrm{trap}})}\right)(z^{\mathrm{trap}})^{-1}+1},$$
$$z^{\mathrm{trap}}(\tau^{\mathrm{trap}}) = -\mathrm{Li}_3^{-1}\left(-\frac{F_0(\tau^{\mathrm{trap}})}{6\bar{T}^3(\tau^{\mathrm{trap}})}\right). \tag{125}$$

Following a derivation similar to that in Sec. V B 1, we obtain coupled equations for $F_0(\tau^{\mathrm{trap}})$ and $\bar{T}(\tau^{\mathrm{trap}})$:

$$\frac{dF_0}{d\tau^{\mathrm{trap}}} = -I_5F_0^2, \tag{126}$$

$$\frac{d\bar{T}}{d\tau^{\mathrm{trap}}} = \frac{(d\mathcal{E}^{\mathrm{th}}/dF_0)F_0^2I_5 + \mathcal{E}^{\mathrm{th}}F_0I_5 - F_0I_7}{(d\mathcal{E}^{\mathrm{th}}/d\bar{T})}, \tag{127}$$

where

$$I_5 = -\frac{1}{4\pi^4}\int d\theta_1 d\theta_2 d\theta_3 \sin^4\theta_1 d\,\sin^3\theta_2 d\,\sin^2\theta_3 \times \int dR \frac{288\sqrt{\pi}R^5\bar{T}^{3/2}z^{\mathrm{trap}}}{F_0^2[\exp(R^2/\bar{T})+z^{\mathrm{trap}}]} \times \left\{2hR^2\mathrm{Li}_{\frac{3}{2}}\left[-\exp\left(\frac{(h-1)R^2}{\bar{T}}z^{\mathrm{trap}}(\tau^{\mathrm{trap}})\right)\right] + 3\bar{T}\mathrm{Li}_{\frac{3}{2}}\left[-\exp\left(\frac{(h-1)R^2}{\bar{T}}z^{\mathrm{trap}}(\tau^{\mathrm{trap}})\right)\right]\right\} \tag{128}$$

and

$$I_7 = -\frac{1}{12\pi^4}\int d\theta_1 d\theta_2 d\theta_3 \sin^4\theta_1 d\,\sin^3\theta_2 d\,\sin^2\theta_3 \times \int dR \frac{288\sqrt{\pi}R^7\bar{T}^{3/2}z^{\mathrm{trap}}}{F_0^2[\exp(R^2/\bar{T})+z^{\mathrm{trap}}]} \times \left\{2hR^2\mathrm{Li}_{\frac{3}{2}}\left[-\exp\left(\frac{(h-1)R^2}{\bar{T}}z^{\mathrm{trap}}\right)\right] + 3\bar{T}\mathrm{Li}_{\frac{3}{2}}\left[-\exp\left(\frac{(h-1)R^2}{\bar{T}}z^{\mathrm{trap}}\right)\right]\right\}. \tag{129}$$

The necessary expressions for $\mathcal{E}^{\mathrm{th}}$, $d\mathcal{E}^{\mathrm{th}}/dF_0$, and $d\mathcal{E}^{\mathrm{th}}/d\bar{T}$ are also provided below:

$$\mathcal{E}^{\mathrm{th}} = -\frac{6\bar{T}^4\mathrm{Li}_4[-z^{\mathrm{trap}}(\tau^{\mathrm{trap}})]}{F_0}, \tag{130}$$

$$\frac{d\mathcal{E}^{\mathrm{th}}}{dF_0} = \frac{6\bar{T}^4\mathrm{Li}_4[-z^{\mathrm{trap}}(\tau^{\mathrm{trap}})]}{F_0^2} - \frac{1}{6\bar{T}^2\mathrm{Li}_2[-z^{\mathrm{trap}}(\tau^{\mathrm{trap}})]}, \tag{131}$$

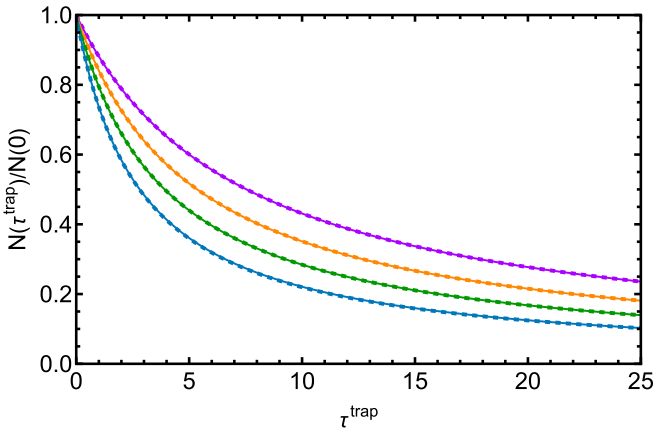

FIG. 9. Particle dynamics obtained from the thermal ansatz, Eqs. (126) and (127) [dashed lines], and directly solving Eq. (120) [solid lines]. From top to bottom, $\bar{T}(0)$ are set to be 2,1,0.5, and 0.1.

$$\frac{d\mathcal{E}^{\rm th}}{d\bar{T}} = \frac{F_0}{2\bar{T}^3 {\rm Li}_2[-z^{\rm trap}(\tau^{\rm trap})]} - \frac{24\bar{T}^4 {\rm Li}_4[-z^{\rm trap}(\tau^{\rm trap})]}{F_0}, \tag{132}$$

Figure 9 presents numerical solutions of particle dynamics from Eqs. (126) and (127). Comparing these results with those from Eq. (120), we find remarkably small differences even in the deep degeneracy regime. This close agreement might suggest that the thermal ansatz is an exact solution to Eq. (120).

However, a careful examination of the radial phase-space distribution $N(R,\tau^{\rm trap}) = R^5\mathcal{F}(R,\tau^{\rm trap})/8$, shown in Fig. 10, reveals a more nuanced picture. For systems starting from high initial temperatures, the profiles remain approximately thermal throughout the evolution. In contrast, for low initial temperatures, despite the particle dynamics appearing similar to those given by the thermal ansatz, the system is, in fact, highly nonequilibrium.

1. High-initial-temperature analytical solution

For high initial temperatures, the integrals in Eqs. (128) and (129) can be explicitly evaluated:

$$I_5 \xrightarrow{\bar{T}\to\infty} \frac{6}{\pi^{7/2}\sqrt{\bar{T}}}\int d\theta_1 d\theta_2 d\theta_3 \sin^4\theta_1 \sin^3\theta_2 \sin^2\theta_3 \frac{(2+h)}{(h-2)^4} = \frac{\mathcal{A}}{\sqrt{\bar{T}}} \simeq \frac{0.190}{\sqrt{\bar{T}}} \tag{133}$$

and

$$I_7 \xrightarrow{\bar{T}\to\infty} \frac{2\sqrt{\bar{T}}}{\pi^{7/2}}\int d\theta_1 d\theta_2 d\theta_3 \sin^4\theta_1 \sin^3\theta_2 \sin^2\theta_3 \frac{(6+5h)}{(h-2)^5} = \mathcal{B}\sqrt{\bar{T}} \simeq 0.175\sqrt{\bar{T}}. \tag{134}$$

Consequently, Eqs. (126) and (127) simplify to

$$\frac{dF_0}{d\tau^{\rm trap}} = -\mathcal{A}F_0^2\bar{T}^{-1/2}, \tag{135}$$

$$\frac{d\bar{T}}{d\tau^{\rm trap}} = (\mathcal{A}-\mathcal{B})F_0\bar{T}^{1/2}. \tag{136}$$

Solving these equations yields

$$F_0(\tau^{\rm trap}) = \frac{1}{\left[1+\frac{(3\mathcal{A}-\mathcal{B})\tau^{\rm trap}}{2\bar{T}(0)^{1/2}}\right]^{2\mathcal{A}/(3\mathcal{A}-\mathcal{B})}}, \tag{137}$$

$$\bar{T}(\tau^{\rm trap}) = \bar{T}(0)\left[1+\frac{(3\mathcal{A}-\mathcal{B})\tau^{\rm trap}}{2\bar{T}(0)^{1/2}}\right]^{2-4\mathcal{A}/(3\mathcal{A}-\mathcal{B})}. \tag{138}$$

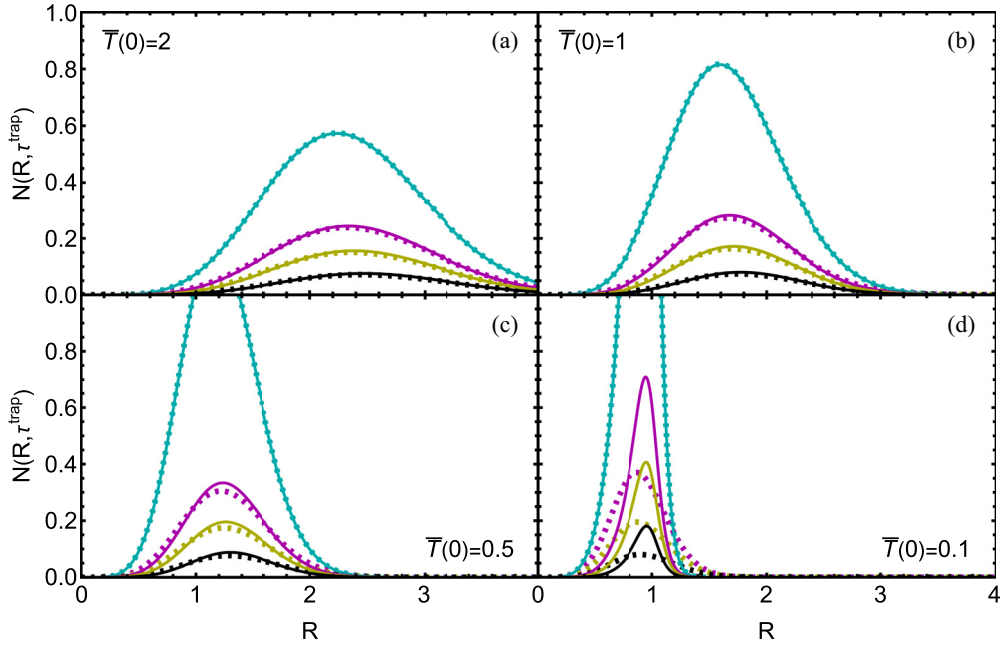

FIG. 10. Comparison between radial phase-space distributions obtained from the thermal ansatz (dotted lines) and by directly solving Eq. (120) (solid lines) at different time shots $\tau^{\rm trap} = 0,\ 10,\ 20$, and 50 denoted by cyan, magenta, yellow, and black colors, respectively.

Notably, Eq. (137) takes the form of Eq. (60), describing an $\mathcal{N}$-body decay with

$$\mathcal{N} = \frac{5\mathcal{A} - \mathcal{B}}{2\mathcal{A}} \simeq 2.041\,67. \tag{139}$$

This result contrasts with our findings in Sec. V A 1, where we demonstrated that for homogeneous systems, $\mathcal{N} = \frac{7}{3}$. This difference underscores the significant impact of flowing dynamics in trapped systems on the two-body dissipation behavior.

VII. SUMMARY

In this companion paper, we present a comprehensive analysis of the inelastic quantum Boltzmann equation (IQBE) for single-component Fermi gases in both free space and harmonic traps. Our approach begins by deriving the IQBE from a non-Hermitian Hamiltonian and demonstrating that elastic collisions play a minimal role in the dynamics of typical experimental systems. For homogeneous systems, we employ the Mellin transform technique to solve the IQBE, revealing that the dissipation follows an $\mathcal{N}$-body decay with a temperature dependent $\mathcal{N}$. This finding challenges the conventional understanding of two-body loss dynamics. To address harmonically trapped systems, we introduce a fast-flowing approximation (FFA) of the IQBE, enabling efficient numerical calculations. This method successfully reproduces experimental data without the need for fitting parameters, validating its efficacy and accuracy. In both free space and trapped scenarios, we compare our calculations with solutions obtained using a thermal ansatz. Our results indicate that the system can achieve a quasithermalized state even in the absence of elastic collisions, except in deeply degenerate regimes. This observation provides new insights into the thermalization processes in these systems.

Our study offers a comprehensive understanding of two-body dissipative behavior in single-component Fermi gases. The results and methodologies presented here serve as valuable benchmarks for calibrating relevant direct simulation Monte Carlo (DSMC) simulations [44]. Furthermore, this work lays the groundwork for extending contact measurements using photoexcitation methods in p-wave BCS-BEC crossover studies.

While this work focuses on the applications of IQBE in the normal phase, recent studies have also shown a growing interest in particle dissipation mechanisms within superfluid regimes [45–53]. The theoretical framework and methodologies developed in this paper can serve as a foundation for future extensions of the inelastic quantum Boltzmann equation into the superfluid regime, potentially offering new insights into the interplay between dissipation and superfluidity.

ACKNOWLEDGMENTS

We would like to acknowledge financial support from the National Natural Science Foundation of China under Grant No. 124B2074 and No. 12204395, Hong Kong RGC Early Career Scheme (Grant No. 24308323), and Collaborative Research Fund (Grant No. C4050-23GF), the Space Application System of China Manned Space Program, and CUHK Direct Grant No. 4053676. We thank D. Blume and K. Lee for their helpful discussions.

APPENDIX A: INELASTIC COLLISION INTEGRAL FROM LINDBLAD EQUATION

In this Appendix, we further provide a more straightforward method of deriving inelastic collision integral (22) starting from the Lindblad master equation. Compared to the time-dependent perturbation method provided in the main text, such a method is advantageous in its rigor, supporting our former derivation, while being inconvenient to obtain the elastic contribution on the same foot.

The Lindblad master equation corresponding to non-Hermitian Hamiltonian (1) is

$$i\hbar\frac{d\rho_t}{dt} = [\hat{T} + \mathrm{Re}(\hat{U}), \rho_t] + i\{\mathrm{Im}(\hat{U}), \rho_t\} - i\sum_{\mathbf{P},m}\hat{L}_{\mathbf{P},m}\rho_t\hat{L}^\dagger_{\mathbf{P},m}, \tag{A1}$$

where the jump operators $\hat{L}_{\mathbf{P},m}$ are defined by Eq. (16) in the main text. By right multiplying $\hat{N}_\mathbf{k} = c^\dagger_\mathbf{k}c_\mathbf{k}$ to both sides of Eq. (A1) and taking trace

$$\begin{aligned} i\hbar\,\mathrm{Tr}\left(\frac{d\rho}{dt}\hat{N}_\mathbf{k}\right) &= i\hbar\frac{d}{dt}\mathrm{Tr}(\rho\hat{N}_\mathbf{k}) \\ &= \mathrm{Tr}([\hat{T} + \mathrm{Re}(\hat{U}), \rho]\hat{N}_\mathbf{k}) + i\,\mathrm{Tr}(\{\mathrm{Im}(\hat{U}), \rho\}\hat{N}_\mathbf{k}) \\ &\quad - i\sum_{\mathbf{P},m}\mathrm{Tr}(\hat{L}_{\mathbf{P},m}\rho\hat{L}^\dagger_{\mathbf{P},m}\hat{N}_\mathbf{k}). \end{aligned} \tag{A2}$$

Using the cyclic property of trace,

$$\mathrm{Tr}([\hat{T} + \mathrm{Re}(\hat{U}), \rho]\hat{N}_\mathbf{k}) = \mathrm{Tr}(\rho[\hat{N}_\mathbf{k}, \hat{T} + \mathrm{Re}(\hat{U})]), \tag{A3}$$

$$\mathrm{Tr}(\{\mathrm{Im}(\hat{U}), \rho\}\hat{N}_\mathbf{k}) = \mathrm{Tr}(\rho\{\hat{N}_\mathbf{k}, \mathrm{Im}(\hat{U})\}), \tag{A4}$$

$$\mathrm{Tr}(\hat{L}_{\mathbf{P},m}\rho\hat{L}^\dagger_{\mathbf{P},m}\hat{N}_\mathbf{k}) = \mathrm{Tr}(\rho\hat{L}^\dagger_{\mathbf{P},m}\hat{N}_\mathbf{k}\hat{L}_{\mathbf{P},m}). \tag{A5}$$

Denoting $\mathrm{Tr}(\rho\hat{A}) = \langle\hat{A}\rangle$,

$$\begin{aligned} i\hbar\frac{d}{dt}\langle\hat{N}_\mathbf{k}\rangle &= \langle[\hat{N}_\mathbf{k}, \hat{T}]\rangle + \langle[\hat{N}_\mathbf{k}, \mathrm{Re}(\hat{U})]\rangle \\ &\quad + i\langle\{\hat{N}_\mathbf{k}, \mathrm{Im}(\hat{U})\}\rangle - i\sum_{\mathbf{P},m}\langle\hat{L}^\dagger_{\mathbf{P},m}\hat{N}_\mathbf{k}\hat{L}_{\mathbf{P},m}\rangle. \end{aligned} \tag{A6}$$

Then we can arrange the right-hand side of Eq. (A6) into normal orders term by term. The first term is

$$\begin{aligned} \langle[\hat{N}_\mathbf{k}, \hat{T}]\rangle &= \sum_\mathbf{q}\frac{\hbar^2q^2}{2m}\langle[\hat{N}_\mathbf{k}, \hat{N}_\mathbf{q}]\rangle \\ &= \sum_\mathbf{q}\frac{\hbar^2q^2}{2m}\delta_{\mathbf{k},\mathbf{q}}(c^\dagger_\mathbf{k}c_\mathbf{q} - c^\dagger_\mathbf{q}c_\mathbf{k}) = 0. \end{aligned} \tag{A7}$$

And the second term,

$$\begin{aligned}\langle[\hat{N}_{\mathbf{k}}, \mathrm{Re}(\hat{U})]\rangle = &\frac{\mathrm{Re}(g)}{2V}\sum_{\mathbf{P},\mathbf{q}',m}\mathcal{V}_m(\mathbf{q}')\mathcal{V}_m^*\left(\mathbf{k}-\tfrac{\mathbf{P}}{2}\right)\left\langle c_{\mathbf{k}}^\dagger c_{\mathbf{P}-\mathbf{k}}^\dagger c_{\frac{\mathbf{P}}{2}-\mathbf{q}'}c_{\frac{\mathbf{P}}{2}+\mathbf{q}'}\right\rangle\\ &+\frac{\mathrm{Re}(g)}{2V}\sum_{\mathbf{P},\mathbf{q}',m}\mathcal{V}_m(\mathbf{q}')\mathcal{V}_m^*\left(\tfrac{\mathbf{P}}{2}-\mathbf{k}\right)\left\langle c_{\mathbf{P}-\mathbf{k}}^\dagger c_{\mathbf{k}}^\dagger c_{\frac{\mathbf{P}}{2}-\mathbf{q}'}c_{\frac{\mathbf{P}}{2}+\mathbf{q}'}\right\rangle\\ &+\frac{\mathrm{Re}(g)}{2V}\sum_{\mathbf{P},\mathbf{q},m}\mathcal{V}_m\left(\tfrac{\mathbf{P}}{2}-\mathbf{k}\right)\mathcal{V}_m^*(\mathbf{q})\left\langle c_{\frac{\mathbf{P}}{2}-\mathbf{q}}^\dagger c_{\frac{\mathbf{P}}{2}+\mathbf{q}}^\dagger c_{\mathbf{k}}c_{\mathbf{P}-\mathbf{k}}\right\rangle\\ &+\frac{\mathrm{Re}(g)}{2V}\sum_{\mathbf{P},\mathbf{q},m}\mathcal{V}_m\left(\mathbf{k}-\tfrac{\mathbf{P}}{2}\right)\mathcal{V}_m^*(\mathbf{q})\left\langle c_{\frac{\mathbf{P}}{2}-\mathbf{q}}^\dagger c_{\frac{\mathbf{P}}{2}+\mathbf{q}}^\dagger c_{\mathbf{P}-\mathbf{k}}c_{\mathbf{k}}\right\rangle,\end{aligned}\tag{A8}$$

where we define $\mathcal{V}_m(\mathbf{q}) = 2\sqrt{\pi}Y_{1m}(\hat{\mathbf{q}})q$ for convenience. It is noted that $\mathcal{V}_m(\mathbf{q}) = -\mathcal{V}_m(-\mathbf{q})$. By changing dummy integral variable $\mathbf{q}' \to \mathbf{P}/2 - \mathbf{q}$ in first two summations and $\mathbf{q} \to \mathbf{P}/2 - \mathbf{q}$ in other two summations, we obtain

$$\begin{aligned}\langle[\hat{N}_{\mathbf{k}}, \mathrm{Re}(\hat{U})]\rangle = &-\frac{\mathrm{Re}(g)}{V}\sum_{\mathbf{P},\mathbf{q},m}\mathcal{V}_m\left(\mathbf{q}-\tfrac{\mathbf{P}}{2}\right)\mathcal{V}_m^*\left(\mathbf{k}-\tfrac{\mathbf{P}}{2}\right)\langle c_{\mathbf{k}}^\dagger c_{\mathbf{P}-\mathbf{k}}^\dagger c_{\mathbf{q}}c_{\mathbf{P}-\mathbf{q}}\rangle\\ &+\frac{\mathrm{Re}(g)}{V}\sum_{\mathbf{P},\mathbf{q},m}\mathcal{V}_m\left(\mathbf{q}-\tfrac{\mathbf{P}}{2}\right)\mathcal{V}_m^*\left(\mathbf{k}-\tfrac{\mathbf{P}}{2}\right)\langle c_{\mathbf{q}}^\dagger c_{\mathbf{P}-\mathbf{q}}^\dagger c_{\mathbf{k}}c_{\mathbf{P}-\mathbf{k}}\rangle.\end{aligned}\tag{A9}$$

Because $c_{\mathbf{q}}^\dagger c_{\mathbf{P}-\mathbf{q}}^\dagger c_{\mathbf{k}}c_{\mathbf{P}-\mathbf{k}} = (c_{\mathbf{k}}^\dagger c_{\mathbf{P}-\mathbf{k}}^\dagger c_{\mathbf{q}}c_{\mathbf{P}-\mathbf{q}})^\dagger$,

$$-\langle c_{\mathbf{k}}^\dagger c_{\mathbf{P}-\mathbf{k}}^\dagger c_{\mathbf{q}}c_{\mathbf{P}-\mathbf{q}}\rangle + \langle c_{\mathbf{q}}^\dagger c_{\mathbf{P}-\mathbf{q}}^\dagger c_{\mathbf{k}}c_{\mathbf{P}-\mathbf{k}}\rangle = -\langle c_{\mathbf{k}}^\dagger c_{\mathbf{P}-\mathbf{k}}^\dagger c_{\mathbf{q}}c_{\mathbf{P}-\mathbf{q}}\rangle + \langle c_{\mathbf{k}}^\dagger c_{\mathbf{P}-\mathbf{k}}^\dagger c_{\mathbf{q}}c_{\mathbf{P}-\mathbf{q}}\rangle^*.\tag{A10}$$

Then,

$$\langle[\hat{N}_{\mathbf{k}}, \mathrm{Re}(\hat{U})]\rangle = -\frac{2i\,\mathrm{Re}(g)}{V}\sum_{\mathbf{P},\mathbf{q},m}\mathcal{V}_m\left(\mathbf{q}-\frac{\mathbf{P}}{2}\right)\mathcal{V}_m^*\left(\mathbf{k}-\frac{\mathbf{P}}{2}\right)\mathrm{Im}\langle c_{\mathbf{k}}^\dagger c_{\mathbf{P}-\mathbf{k}}^\dagger c_{\mathbf{q}}c_{\mathbf{P}-\mathbf{q}}\rangle.\tag{A11}$$

Following almost the same procedure, the third term is evaluated to

$$\begin{aligned}i\langle\{\hat{N}_{\mathbf{k}}, \mathrm{Im}(\hat{U})\}\rangle = &-\frac{2i\,\mathrm{Im}(g)}{V}\sum_{\mathbf{P},\mathbf{q},m}\mathcal{V}_m\left(\mathbf{q}-\frac{\mathbf{P}}{2}\right)\mathcal{V}_m^*\left(\mathbf{k}-\frac{\mathbf{P}}{2}\right)\mathrm{Re}\langle c_{\mathbf{k}}^\dagger c_{\mathbf{P}-\mathbf{k}}^\dagger c_{\mathbf{q}}c_{\mathbf{P}-\mathbf{q}}\rangle\\ &+\frac{2i\,\mathrm{Im}(g)}{V}\sum_{\mathbf{P},\mathbf{q},\mathbf{q}',m}\mathcal{V}_m(\mathbf{q})\mathcal{V}_m^*(\mathbf{q}')\langle c_{\frac{\mathbf{P}}{2}+\mathbf{q}}^\dagger c_{\frac{\mathbf{P}}{2}-\mathbf{q}}^\dagger c_{\mathbf{k}}^\dagger c_{\mathbf{k}}c_{\frac{\mathbf{P}}{2}-\mathbf{q}'}c_{\frac{\mathbf{P}}{2}+\mathbf{q}'}\rangle.\end{aligned}\tag{A12}$$

It can be observed that the fourth term in Eq. (A6) has already been in the normal order and is exactly opposite to the last line of Eq. (A12). Substituting the above expressions back to Eq. (A6), we have

$$\frac{d\langle\hat{N}_{\mathbf{k}}\rangle}{dt} = -\frac{2}{\hbar V}\sum_{\mathbf{P},\mathbf{q},m}\mathcal{V}_m\left(\frac{\mathbf{P}}{2}-\mathbf{k}\right)\mathcal{V}_m^*\left(\frac{\mathbf{P}}{2}-\mathbf{q}\right)[\mathrm{Re}(g)\mathrm{Im}\langle c_{\mathbf{k}}^\dagger c_{\mathbf{P}-\mathbf{k}}^\dagger c_{\mathbf{P}-\mathbf{q}}c_{\mathbf{q}}\rangle + \mathrm{Im}(g)\mathrm{Re}\langle c_{\mathbf{k}}^\dagger c_{\mathbf{P}-\mathbf{k}}^\dagger c_{\mathbf{P}-\mathbf{q}}c_{\mathbf{q}}\rangle].\tag{A13}$$

From now on, we will work in the weakly interacting and weakly reactive regimes, i.e., $\mathrm{Re}(g)$ and $\mathrm{Im}(g)$ are small enough to treat g as a perturbative parameter. Under the first-order perturbation, four-operator expectation can be factored into a multiplication of several $\langle\hat{N}_{\mathbf{k}}\rangle$ [33]. Since Eq. (A13) itself already has a first-order coupling, the first-order perturbation of the expression is nothing but the noninteracting limit of four-operator expectations, which is

$$\begin{aligned}\langle c_{\mathbf{k}}^\dagger c_{\mathbf{P}-\mathbf{k}}^\dagger c_{\mathbf{P}-\mathbf{q}}c_{\mathbf{q}}\rangle &\to (\delta_{\mathbf{q},\mathbf{k}} - \delta_{\mathbf{P},\mathbf{q}+\mathbf{k}})\langle c_{\mathbf{k}}^\dagger c_{\mathbf{P}-\mathbf{k}}^\dagger c_{\mathbf{P}-\mathbf{k}}c_{\mathbf{k}}\rangle\\ &\to (\delta_{\mathbf{q},\mathbf{k}} - \delta_{\mathbf{P},\mathbf{q}+\mathbf{k}})\langle\hat{N}_{\mathbf{k}}\rangle\langle\hat{N}_{\mathbf{P}-\mathbf{k}}\rangle.\end{aligned}\tag{A14}$$

It is worth noting that one should not directly write the second step of Eq. (A14) because

$$\begin{aligned}\langle c_{\mathbf{k}}^\dagger c_{\mathbf{P}-\mathbf{k}}^\dagger c_{\mathbf{P}-\mathbf{k}}c_{\mathbf{k}}\rangle &= \langle c_{\mathbf{k}}^\dagger c_{\mathbf{k}}c_{\mathbf{P}-\mathbf{k}}^\dagger c_{\mathbf{P}-\mathbf{k}}\rangle - \delta_{\mathbf{k},\mathbf{P}-\mathbf{k}}\langle c_{\mathbf{k}}^\dagger c_{\mathbf{P}-\mathbf{k}}\rangle\\ &\approx \langle N_{\mathbf{k}}\rangle\langle N_{\mathbf{P}-\mathbf{k}}\rangle - \delta_{\mathbf{k},\mathbf{P}/2}\langle N_{\mathbf{k}}\rangle,\end{aligned}\tag{A15}$$

one finds an additional one-body term contributes. The reason why it can be ignored when Eq. (A15) is substituted into Eq. (A13), the one-body term always appears with $\mathcal{V}_{1m}(0) = 0$.

It can be understood that the $\delta_{\mathbf{P},\mathbf{q}+\mathbf{k}}$ contribution is trivial, and the $\delta_{\mathbf{q},\mathbf{k}}$ term describes the momentum exchange of two incoming particles. The consequence of taking the

noninteracting limit is that the collision part in Eq. (A13) would completely disappear as four-operator terms in the middle of Eq. (A14) are all Hermitian with purely real expectation.

Substituting Eq. (A14) into (A13), we obtain

$$\frac{d\langle\hat{N}_{\mathbf{k}}\rangle}{dt} = -\frac{2\,\mathrm{Im}(g)}{\hbar V}\sum_{\mathbf{q},m}\mathcal{V}_m\left(\frac{\mathbf{q}-\mathbf{k}}{2}\right)\mathcal{V}_m^*\left(\frac{\mathbf{k}-\mathbf{q}}{2}\right) \times [\langle\hat{N}_{\mathbf{k}}\rangle\langle\hat{N}_{\mathbf{q}}\rangle - \langle\hat{N}_{\mathbf{k}}\rangle\langle\hat{N}_{\mathbf{P}-\mathbf{k}}\rangle]. \tag{A16}$$

Changing variable $\mathbf{P}\to\mathbf{k}+\mathbf{q}$ in the second summation above, we finally reach the same form as Eq. (21) in the main text:

$$\frac{d\langle\hat{N}_{\mathbf{k}}\rangle}{dt} = \frac{4\,\mathrm{Im}(g)}{\hbar V}\sum_{\mathbf{q},m}\left|\mathcal{V}_m\left(\frac{\mathbf{q}-\mathbf{k}}{2}\right)\right|^2\langle\hat{N}_{\mathbf{k}}\rangle\langle\hat{N}_{\mathbf{q}}\rangle$$

$$\to \frac{dN_{\mathbf{k}}}{dt} = \frac{3\,\mathrm{Im}(g)}{\hbar V}\int\frac{d^3q}{(2\pi)^3}(\mathbf{q}-\mathbf{k})^2N_{\mathbf{k}}N_{\mathbf{q}}, \tag{A17}$$

where $\langle\hat{N}_{\mathbf{k}}\rangle = N_{\mathbf{k}}d^3k$ and we used Unsöld theorem for $l=1$:

$$\sum_m\left|\mathcal{V}_m\left(\frac{\mathbf{q}-\mathbf{k}}{2}\right)\right|^2 = 4\pi\left(\frac{\mathbf{q}-\mathbf{k}}{2}\right)^2\sum_m\hat{Y}_{1m}^2\left(\frac{\mathbf{q}-\mathbf{k}}{|\mathbf{q}-\mathbf{k}|}\right) = \frac{3}{4}(\mathbf{q}-\mathbf{k})^2. \tag{A18}$$

APPENDIX B: SHORT-TIME DYNAMICS AND INITIAL LOSS RATES

The short-time ($t\to 0$) limit of our IQBE framework provides a direct connection to experimentally measured initial loss rates. Taking $t\to 0$ in our formalism, $n_{\mathbf{k}}$ and $n_{\mathbf{q}}$ in inelastic collision integral (22) are simply replaced by Fermi-Dirac distribution [Eq. (41)]. By defining the initial loss rate β to be

$$\frac{dn}{dt} = -\beta n^2, \tag{B1}$$

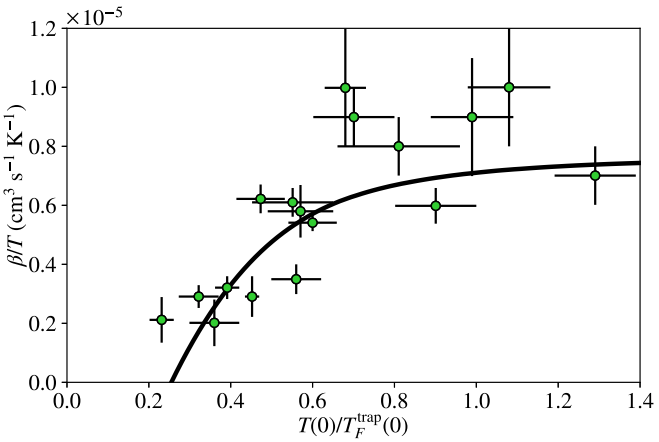

FIG. 11. Comparison between experimental data (green symbols) from Ref. [26] and theoretical predictions (black solid line) for the temperature-dependent loss rate coefficient β with $\mathrm{Im}(v_p) = (118a_0)^3$.

where the density $n = \int d^3k/(2\pi)^3 n_{\mathbf{k}}$, it is straightforward to find

$$\beta = \frac{-144\pi^2\hbar\,\mathrm{Im}(v_p)\mathrm{Li}_{\frac{5}{2}}(-z)}{M\lambda_T^2\mathrm{Li}_{\frac{3}{2}}(-z)} \tag{B2}$$

with $\lambda_T = \hbar\sqrt{\frac{2\pi}{Mk_BT}}$ the thermal wavelength.

For harmonically trapped systems, a systematic procedure accounting for the trap geometry and excluding the antievaporation effect is necessary for comparison with standard experimental measurement. Under similar data processing as in Ref. [54], Eq. (B2) can be converted to the result of Fig. 11. Figure 11 demonstrates the excellent agreement between our theoretical predictions and experimental measurements from Ref. [26]. Compared with previous results presented in Ref. [54], theoretical prediction in Fig. 11 is more accurate since it is converted from an exact expression without any interpolation.

[1] K. Huang, *Statistical Mechanics* (Wiley, Hoboken, NJ, 2008).

[2] E. Zaremba, T. Nikuni, and A. Griffin, Dynamics of trapped Bose gases at finite temperatures, J. Low Temp. Phys. **116**, 277 (1999).

[3] M. Urban and P. Schuck, Dynamics of a trapped Fermi gas in the BCS phase, Phys. Rev. A **73**, 013621 (2006).

[4] M. Urban, Coupling of hydrodynamics and quasiparticle motion in collective modes of superfluid trapped Fermi gases, Phys. Rev. A **75**, 053607 (2007).

[5] G. Puppo, Kinetic models of BGK type and their numerical integration, Riv. Mat. Univ. Parma, **10**, 299 (2019).

[6] L. You and M. Holland, Ballistic expansion of trapped thermal atoms, Phys. Rev. A **53**, R1 (1996).

[7] D. Guéry-Odelin, Mean-field effects in a trapped gas, Phys. Rev. A **66**, 033613 (2002).

[8] D. Guéry-Odelin, F. Zambelli, J. Dalibard, and S. Stringari, Collective oscillations of a classical gas confined in harmonic traps, Phys. Rev. A **60**, 4851 (1999).

[9] P. Pedri, D. Guéry-Odelin, and S. Stringari, Dynamics of a classical gas including dissipative and mean-field effects, Phys. Rev. A **68**, 043608 (2003).

[10] T. Nikuni, J. E. Williams, and C. W. Clark, Linear spin waves in a trapped Bose gas, Phys. Rev. A **66**, 043411 (2002).

[11] G. A. Bird, *Molecular Gas Dynamics And The Direct Simulation Of Gas Flows* (Oxford University Press, Oxford, 1994).

[12] L. Pareschi and G. Russo, An introduction to Monte Carlo method for the Boltzmann equation, ESAIM: Proc. **10**, 35 (2001).

[13] H. Wu and C. J. Foot, Direct simulation of evaporative cooling, J. Phys. B: At. Mol. Phys. **29**, L321 (1996).

[14] B. Jackson and E. Zaremba, Modeling Bose-Einstein condensed gases at finite temperatures with N-body simulations, Phys. Rev. A **66**, 033606 (2002).

[15] T. Lepers, D. Davesne, S. Chiacchiera, and M. Urban, Numerical solution of the Boltzmann equation for the collective modes of trapped Fermi gases, Phys. Rev. A **82**, 023609 (2010).

[16] P. Barletta, J. Tennyson, and P. F. Barker, Direct Monte Carlo simulation of the sympathetic cooling of trapped molecules by ultracold argon atoms, New J. Phys. **12**, 113002 (2010).

[17] A. C. J. Wade, D. Baillie, and P. B. Blakie, Direct simulation Monte Carlo method for cold-atom dynamics: Classical Boltzmann equation in the quantum collision regime, Phys. Rev. A **84**, 023612 (2011).

[18] S. Ospelkaus, K.-K. Ni, D. Wang, M. H. G. De Miranda, B. Neyenhuis, . G. Quéméner, P. S. Julienne, J. L. Bohn, D. S. Jin, and J. Ye, Quantum-state controlled chemical reactions of ultracold potassium-rubidium molecules, Science **327**, 853 (2010).

[19] N. Sela and I. Goldhirsch, Hydrodynamic equations for rapid flows of smooth inelastic spheres, to Burnett order, J. Fluid Mech. **361**, 41 (1998).

[20] V. Garzó and J. W. Dufty, Dense fluid transport for inelastic hard spheres, Phys. Rev. E **59**, 5895 (1999).

[21] E. Ben-Naim, S. Y. Chen, G. D. Doolen, and S. Redner, Shocklike dynamics of inelastic gases, Phys. Rev. Lett. **83**, 4069 (1999).

[22] A. V. Bobylev, J. A. Carrillo, and I. M. Gamba, On some properties of kinetic and hydrodynamic equations for inelastic interactions, J. Stat. Phys. **98**, 743 (2000).

[23] E. Ben-Naim and P. L. Krapivsky, Scaling, multiscaling, and nontrivial exponents in inelastic collision processes, Phys. Rev. E **66**, 011309 (2002).

[24] L. Pan, X. Chen, Y. Chen, and H. Zhai, Non-Hermitian linear response theory, Nat. Phys. **16**, 767 (2020).

[25] X.-Y. Gao and Y. Yan, companion paper, Fate of thermalization of ultracold fermions with two-body dissipation, Phys. Rev. Lett. **134**, 153402 (2025).

[26] L. De Marco, G. Valtolina, K. Matsuda, W. G. Tobias, J. P. Covey, and J. Ye, A degenerate Fermi gas of polar molecules, Science **363**, 853 (2019).

[27] M. Duda, X.-Y. Chen, R. Bause, A. Schindewolf, I. Bloch, and X.-Y. Luo, Long-lived fermionic feshbach molecules with tunable p-wave interactions, Phys. Rev. A **107**, 053322 (2023).

[28] E. Braaten, H.-W. Hammer, and G. P. Lepage, Lindblad equation for the inelastic loss of ultracold atoms, Phys. Rev. A **95**, 012708 (2017).

[29] C. Ticknor, C. A. Regal, D. S. Jin, and J. L. Bohn, Multiplet structure of Feshbach resonances in nonzero partial waves, Phys. Rev. A **69**, 042712 (2004).

[30] C. Luciuk, S. Trotzky, S. Smale, Z. Yu, S. Zhang, and J. H. Thywissen, Evidence for universal relations describing a gas with p-wave interactions, Nat. Phys. **12**, 599 (2016).

[31] A. L. Fetter and J. D. Walecka, *Quantum Theory of Many-Particle Systems* (Dover, New York, 2012).

[32] D. W. Snoke, G. Liu, and S. M. Girvin, The basis of the Second Law of thermodynamics in quantum field theory, Ann. Phys. **327**, 1825 (2012).

[33] P. He, T. Bilitewski, C. H. Greene, and A. M. Rey, Exploring chemical reactions in a quantum degenerate gas of polar molecules via complex formation, Phys. Rev. A **102**, 063322 (2020).

[34] C.-H. Huang, T. Giamarchi, and M. A. Cazalilla, Modeling particle loss in open systems using Keldysh path integral and second order cumulant expansion, Phys. Rev. Res. **5**, 043192 (2023).

[35] J. Maki, L. Rosso, L. Mazza, and A. Biella, Loss-induced collective mode in one-dimensional Bose gases, Phys. Rev. A **110**, 043315 (2024).

[36] Z. Idziaszek and P. S. Julienne, Universal rate constants for reactive collisions of ultracold molecules, Phys. Rev. Lett. **104**, 113202 (2010).

[37] D. A. Butts and D. S. Rokhsar, Trapped Fermi gases, Phys. Rev. A **55**, 4346 (1997).

[38] C. R. Monroe, E. A. Cornell, C. A. Sackett, C. J. Myatt, and C. E. Wieman, Measurement of Cs-Cs Elastic scattering at $T = 30\,\mu$K, Phys. Rev. Lett. **70**, 414 (1993).

[39] D. Wood, The Computation of polylogarithms, Technical Report No. 15-92*, University of Kent, Computing Laboratory, University of Kent, Canterbury, UK, 1992.

[40] N. P. Mehta, S. T. Rittenhouse, J. P. D'Incao, J. von Stecher, and C. H. Greene, General theoretical description of N-body recombination, Phys. Rev. Lett. **103**, 153201 (2009).

[41] H. Bateman, A. Erdélyi, W. Magnus, and F. Oberhettinger, *Tables of Integral Transforms* (McGraw-Hill, New York, 1954), Vol. 1.

[42] K.-K. Ni, S. Ospelkaus, D. Wang, G. Quéméner, B. Neyenhuis, M. H. G. de Miranda, J. L. Bohn, J. Ye, and D. S. Jin, Dipolar collisions of polar molecules in the quantum regime, Nature (London) **464**, 1324 (2010).

[43] B. Zhu, G. Quéméner, A. M. Rey, and M. J. Holland, Evaporative cooling of reactive polar molecules confined in a two-dimensional geometry, Phys. Rev. A **88**, 063405 (2013).

[44] R. R. W. Wang, S. Biswas, S. Eppelt, F. Deng, X.-Y. Luo, and J. L. Bohn, Simulations of evaporation to deep Fermi degeneracy in microwave-shielded molecules, Phys. Rev. A **110**, 043309 (2024).

[45] K. Yamamoto, M. Nakagawa, K. Adachi, K. Takasan, M. Ueda, and N. Kawakami, Theory of non-Hermitian fermionic superfluidity with a complex-valued interaction, Phys. Rev. Lett. **123**, 123601 (2019).

[46] K. Yamamoto, M. Nakagawa, N. Tsuji, M. Ueda, and N. Kawakami, Collective excitations and nonequilibrium phase transition in dissipative fermionic superfluids, Phys. Rev. Lett. **127**, 055301 (2021).

[47] C. Wang, C. Liu, and Z.-Y. Shi, Complex contact interaction for systems with short-range two-body losses, Phys. Rev. Lett. **129**, 203401 (2022).

[48] X.-D. Dai, F. Song, and Z. Wang, Solvable BCS-Hubbard Liouvillians in arbitrary dimensions, Phys. Rev. B **108**, 115127 (2023).

[49] H. Li, X.-H. Yu, M. Nakagawa, and M. Ueda, Yang-Lee zeros, semicircle theorem, and nonunitary criticality in bardeen-cooper-schrieffer superconductivity, Phys. Rev. Lett. **131**, 216001 (2023).

[50] G. Mazza and M. Schirò, Dissipative dynamics of a fermionic superfluid with two-body losses, Phys. Rev. A **107**, L051301 (2023).

[51] T. Shi, S. Wang, Z. Zheng, and W. Zhang, Two-dimensional non-Hermitian fermionic superfluidity with spin imbalance, Phys. Rev. A **109**, 063306 (2024).

[52] S. Takemori, K. Yamamoto, and A. Koga, Theory of non-Hermitian fermionic superfluidity on a honeycomb lattice: Interplay between exceptional manifolds and Van Hove singularity, Phys. Rev. B **109**, L060501 (2024).

[53] H. Li, X.-H. Yu, M. Nakagawa, and M. Ueda, Dissipative superfluidity in a molecular Bose-Einstein condensate, arXiv:2406.08868.

[54] X.-Y. Gao, D. Blume, and Y. Yan, Temperature-dependent contact of weakly interacting single-component Fermi gases and loss rate of degenerate polar molecules, Phys. Rev. Lett. **131**, 043401 (2023).